

UCLA

UCLA Electronic Theses and Dissertations

Title

Electrochemical and Design Optimization of Battlet-based Flexible Li-ion Batteries on FlexTrate™

Permalink

<https://escholarship.org/uc/item/0013w7f2>

Author

Sheth, Mansi Sunil

Publication Date

2025

Peer reviewed|Thesis/dissertation

UNIVERSITY OF CALIFORNIA

Los Angeles

Electrochemical and Design Optimization of Battlet-based Flexible Li-ion Batteries on
FlexTrate™

A thesis submitted in partial satisfaction
of the requirement for degree Master of Science
in Material Science and Engineering

by

Mansi Sunil Sheth

2025

@ Copyright by

Mansi Sunil Sheth

2025

ABSTRACT OF THE THESIS

Electrochemical and Design Optimization of Battlet-based Flexible Li-ion Batteries on FlexTrate™

by

Mansi Sunil Sheth

Master of Science in Materials Science and Engineering

University of California, Los Angeles, 2025

Subramanian Srikanteswara Iyer, Chair

Recent advancements in biomedical wearable devices have significantly improved miniaturization, flexibility, and sensitivity. However, power delivery systems remain a critical bottleneck due to bulky and rigid commercial lithium-ion batteries, which degrade under mechanical deformation and limit device flexibility, safety, and form factor. To address these challenges, flexible battery technologies such as pouch cells, rubber-like batteries, and 1D fibrous batteries have been explored. Pouch cells, while commercially viable, are constrained by limited bending radii (~20 mm), flammable electrolytes, and issues like leakage and swelling. Rubber-like batteries offer stretchability but suffer from low ionic conductivity and high internal resistance. Similarly, 1D fibrous batteries enable integration into fabrics but face limitations in energy and power density.

To overcome these limitations, we propose two novel battery architectures: the battlet design and the interdigitated battlet design, aimed at enhancing both mechanical and electrochemical performance for flexible lithium-ion batteries. These designs seek to provide improved flexibility, energy density, and form adaptability suitable for next-generation wearable electronics. In addition, we incorporate an ionic liquid-based electrolyte to address the safety hazards posed by traditional organic electrolytes. Ionic liquids, being room-temperature molten salts, offer key advantages such as nonflammability, low volatility, high thermal stability, and wide electrochemical stability windows (4.5–5 V). These properties make them ideal for enhancing battery safety in wearable applications.

Through these design innovations and material choices, our work aims to achieve a new class of intrinsically safe, high-performance, and mechanically robust flexible batteries tailored for wearable electronics.

The thesis of Mansi Sunil Sheth is approved.

Bruce S. Dunn

Qibing Pei

Subramanian S Iyer, Committee Chair

University of California Los Angeles

2025

To my parents

TABLE OF CONTENTS

CHAPTER 1 INTRODUCTION AND BACKGROUND	1
1.1 Motivation	1
1.2 Fundamentals of Li-ion Batteries	2
1.2.1 Cathode and Anode Materials in Li-ion Batteries	3
1.2.2 Solid Electrolyte Interface (SEI)	8
1.2.3 Battery Parameters and Electrochemical Cycling Test Procedure	10
1.3 Electrolyte Types in Li-ion Batteries	12
1.4 Organization of This Work	17
CHAPTER 2 FABRICATION OF THE BATTLET ELECTRODE	19
2.1 Battlet Electrode Fabrication Process	20
2.2 Comparison of Stencil Printing and Ink-Jet Printing Technology	27
2.2.1 Electrode Preparation for Electrochemical Testing	31
CHAPTER 3 ELECTROCHEMICAL STUDY	33
3.1 Selection of Additive for Optimal Anode Performance.....	33
3.2 Initial Electrochemical Study of LFP/Gr Battlet Full Cell in Ionic Liquid Electrolyte	36
3.3 Effect of Salt Concentration (LiFSI) in Ionic Liquid Electrolyte on the Cycling Performance of Li-ion Battery.....	42
3.4 Effect of Cation Type in the Solvent of the Ionic Liquid Electrolyte on the Cycling Performance of Battlet Li-ion Battery.....	47

CHAPTER 4 BATTLET INTERDIGITATED CO-PLANAR LI-ION BATTERY

4.1	Motivation for the Development of Co-Planar Interdigitated Li-ion Battery.....	52
4.2	Fabrication of Interdigitated Battlet Co-planar Battery on Flexible Substrate	56
4.3	Electrochemical Cycling Results	60
CHAPTER 5 CONCLUSION AND PERSPECTIVE		64
REFERENCES		65

LIST OF FIGURES

Figure 1-1: Components of traditional Li-ion battery during discharge	3
Figure 1-2: Classification of cathode materials used in Li-ion batteries	4
Figure 1-3: Classification of anode materials used in Li-ion batteries; Stages of lithium intercalation into graphite at various voltages	6
Figure 1-4: (a)Galvanostatic charging and discharging cycle of graphite with lithium metal as counter electrode and reference for the first (top) and second (bottom) cycle ; (b)The potential range of electrolyte stability, compared to the potentials of common electrode materials.....	9
Figure 1-5: (a) Cathode half-cell configuration shown in a split cell; (b) Anode half-cell configuration shown in a split cell; (c) Cathode and anode half cycle charge/discharge curves	12
Figure 2-1: (a) Comparison of the conventional planar structure and the Battlet structure; (b)battlet electrode before bending; (c) Battlet electrode after bending	20
Figure 2-2: Fabrication process of the battlet flexible Li-ion battery	21
Figure 2-3: Interactions of materials in the electrodes (left); SEM image at 1400x of cathode electrode showing the LFP particles being held together by PVDF particles	22
Figure 2-4: (a)Stencil Printing method (b) Ink-jet printing method	23
Figure 2-5: Methods to maintain optimal N/P ratio in LFP/Gr cell	24
Figure 2-6: Optical images of cathode and anode battlet using (a) Stencil printing (b) Ink-jet printer; Confocal microscope images of the surface profile of cathode electrode using (c) stencil printing and (d) Ink-jet printer	25
Figure 2-7: SEM images of (a) cathode battlet surface at corner (b) zoom on image of cathode at 4000x (c) anode battlet surface at corner (d) zoom in image of anode at 4000x	27

Figure 2-8: Structure model of LFP Electrode	28
Figure 2-9: Variation of electrode thickness with different slurry composition and stencil thickness	29
Figure 2-10: Comparison of theoretical and tested electrode capacity at different electrode composition and thickness	30
Figure 2-11: Optical images of dried LFP electrode surface fabricated using different slurry compositions and stencil thickness	31
Figure 3-1: Additives used in Li-ion batteries	34
Figure 3-2: Charge/Discharge cycling at different C rate of anode half cells in organic electrolyte with (a) VC additive (b) FEC additive	35
Figure 3-3: Charge/Discharge cycling at different C rate of anode half cells in LiFSI:PYR ₁₄ FSI 2:3 ionic liquid electrolyte with (a)VC additive (b) FEC additive	35
Figure 3-4: Charge/Discharge curves of cathode half-cell at different C rates in (a) organic liquid electrolyte and (b) ionic liquid electrolyte. Increase in polarization with increasing C-rate indicated by arrows	37
Figure 3-5: Charge/Discharge curves of anode half cells at different C rates in (a) Organic electrolyte (b) ionic liquid electrolyte	38
Figure3-6: Charge/Discharge curves of LFP/Gr full cells in (a) organic electrolyte (cell capacity 1.2 mAh/cm ²) (b)ionic liquid electrolyte (cell capacity 1.2 mAh/cm ²) (c) ionic liquid electrolyte (lower cell capacity 0.8 mAh/cm ²)	40
Figure 3-7: %Capacity retention comparison at various C-rates for ionic liquid electrolyte and ionic liquid electrolyte	41

Figure 3-8: Charge/discharge of anode half-cell in IL electrolyte (a) LiFSI: EmimFSI 2:3 + 5%FEC (b) LiFSI: EmimFSI 1:9 + 5%FEC	44
Figure 3-9: %Capacity retention comparison at various C-rates for HCE and LCE ionic liquid electrolyte with Pyr14 ⁺ and Emim ⁺ cation containing ionic liquid	45
Figure 3-10: Solvation structure of Li ⁺ in case of HCE and LCE. Demonstration of solvent co-intercalation into graphite in case of low concentration electrolyte (LCE)	46
Figure 3-11: Opened anode half cells cycled in low salt concentration IL electrolyte (right) and high salt concentration IL electrolyte (left)	47
Figure 3-12: Charge/discharge curve of anode half-cell in (a)LiFSI: EmimFSI 2:3 IL electrolyte (b)LiFSI: PYR ₁₄ FSI 2:3 IL electrolyte	48
Figure 3-13: Comparison of (a) areal capacity (b)cycling performance of LFP/Gr full cell in Emim and Pyr14 based ionic liquid electrolyte	50
Figure 4-1: (a) Misalignment of the co-facial electrodes causing formation and growth of Li dendrites over time; (b) shorting of battery due to puncture of separator by the Li dendrites	52
Figure 4-2: (a)-(c) Li ⁺ ion diffusion path in cofacial and coplanar electrode design; (d) structure of proposed battlet interdigitated electrode	56
Figure 4-3: Fabrication process flow for interdigitated current collectors	58
Figure 4-4: (a) Configuration of interdigitated current collectors and battlet electrodes (b) optical image of battlet electrodes (c) Confocal microscope images of the surface profile of interdigitated battlet electrode	59
Figure 4-5: Charge/discharge cycle of LFP/LTO interdigitated battery in (a) organic electrolyte (b) ionic liquid electrolyte	61

Figure 4-6: Charge/Discharge cycle of LFP/LTO battlet interdigitated battery in (a) organic electrolyte (b) ionic liquid electrolyte	62
Figure 4-7: % capacity retention in LFP/LTO battlet interdigitated cell in ionic liquid electrolyte cycled at 0.2C over 20 cycles	62
Figure 4-8: (a) Packaged battery (b) Dynamic Bending (5mm bending radius)	63
Figure 5-1: SEM image (500x) of 4-layer LFP interdigitated electrode printed using direct-ink writing	65

LIST OF TABLES

Table 1-1: Properties of cathode materials used in Li-ion batteries	5
Table 1-2: Properties of anode materials for Li-ion batteries	8
Table 1-3: Variation of charge/discharge current and time at various C rates	10
Table 1-4: Physico-chemical characteristics of battery solvents	14
Table 1-5: Physico-chemical properties of lithium salts used in electrolytes	15
Table 1-6: Classification of cations used in ionic liquids as part of the ionic liquid electrolyte	16
Table 2-1: Design of experiment for optimization of electrode slurry	28
Table 3-1: Physico-Chemical properties IL electrolytes with varying molar concentrations [27][28]	43
Table 4-1: Electrode designs in flexible lithium-ion batteries	55

ACKNOWLEDGEMENTS

First and foremost, I am immensely thankful to my advisor, Prof. Subramanian Iyer, for his guidance, motivation, and expertise throughout this research project. Without his support and vision, this work would not be possible. I would like to extend my heartfelt thanks to the members of my thesis committee, Prof. Bruce Dunn, and Prof. Qibing Pei, for their time, expertise, and valuable input.

I would like to particularly acknowledge and express my sincere gratitude to my fellow CHIPS lab member, Guangqi Ouyang, for his invaluable assistance during the project. Whenever I encountered challenges, he was always there to lend a helping hand and mentored me throughout this project. I am also grateful to Jacky (Tsz Tat) Yu, for his guidance and help on the battery testing which has been instrumental in shaping my thesis. I would also like to extend my sincere appreciation to my colleagues at the CHIPS lab – Randall Irwin, Tanmay Konnur, Henry Sun, Golam Sabbir, Naarendharan, Seungwoo Baek, Michael Yang, Zoe Chen, Vineeth Harish, Jui-Han Liu, Krutikesh Sahoo for their collaborative efforts and assistance. I would also like to thank the staff of UCLA Integrated Systems Nanofabrication Cleanroom, Nanolab Research Facility for their help and support.

Lastly, I am genuinely grateful to my parents Sunil Sheth, Sonal Sheth and sister Nidhi Sheth for their boundless love and encouragement. They have been an endless source of motivation throughout my academic journey. I would also like to thank my friend Nithin Subhash for always being my constant source of support.

CHAPTER 1: INTRODUCTION

1.1 MOTIVATION

In recent years, biomedical wearable devices have achieved much progress in miniaturization, flexibility, and sensitivity. However, current power delivery systems remain too bulky, primarily due to inefficient packaging and integration schemes [1][2]. This bulkiness is partly because commercially available lithium-ion batteries, the industry standard for rigid portable devices, suffer electrochemical degradation under long-term mechanical deformation, such as bending, folding, twisting, and other strain modes. The space allocated for power storage and management is also ever decreasing to make more room for higher functionality. More importantly, the form/shape factor (coin, cylindrical, prismatic, and pouch shapes) of the commercial batteries severely impact the wearable device safety, reliability, flexibility, and miniaturization. Since conventional batteries are not intrinsically flexible, in the past few decades, researchers have developed various types of flexible batteries, including pouch cell batteries [3], rubber-like batteries [4], [5], [6], 1D fibrous batteries [7], [8], [9], etc. Pouch cell batteries are a relatively mature technology in the battery market. While they exhibit some degree of flexibility, they are limited to a bending radius of ~ 20 mm. In addition, pouch cell batteries typically contain flammable organic electrolyte, presenting serious safety concerns for wearable devices. Beyond flammability concerns, other issues, including swelling, leakage, and lack of biocompatibility, limit the application of pouch cells in wearable devices [10]. Other formats such as rubber-like batteries, utilize crosslinked rubber-based polymers to fabricate cathode, anode, and electrolyte, and offer a route for flexible batteries. While this approach provides intrinsic flexibility and stretchability, the ionic conductivity of the electrolyte remains low, resulting in low output power and high internal resistance [3], [11]. 1D fibrous batteries are another emerging type of batteries for

wearable devices. Typically, fibrous cathodes and anodes are weaved together to create a single-thread full-cell battery. This type of 1D batteries can also be woven as a cover for the devices, but with major limitation in energy density and output power density.

To overcome these issues in current designs of flexible batteries, we adopt two new designs 1. Battlet design 2. Interdigitated battlet design to fabricate flexible Li-ion batteries and evaluate if these designs help us meet the current flexible battery requirements in terms of mechanical and electrochemical performance. In addition, an ionic liquid electrolyte is used to address the safety concerns of the Li-ion battery for wearables. Ionic liquids are room-temperature molten salts that exhibit wide electrochemical stability windows (4.5V - 5V), excellent thermal stability, and nonflammability owing to their low vapor pressure [14], [15], [16]. Thus, ionic liquid electrolytes present several advantages over traditional organic electrolytes for powering wearable devices.

1.2 Fundamentals of Li-ion Batteries

In a typical Li-ion battery the positive electrode is called the ‘cathode’ and the negative electrode ‘anode’. These names represent the right naming only when discharging the battery. The role/name is flipped during the charging process of the battery, the positive electrode works as anode and negative electrode works as cathode. This nomenclature came from non-rechargeable primary batteries that never charged. Figure1-1 shows the basic principle of rechargeable Li-ion battery. An ion-conducting electrolyte, containing a dissociated lithium conducting salt is situated between the two electrodes that are separated by a porous membrane called the separator. The separator electrically isolates the two electrodes and only lets the ions pass through. During discharging a battery, the lithium is deintercalated from negative electrode (anode) releasing electrons and gets intercalated into the positive electrode (cathode). During charging, the process is reversed: Li ions migrate from positive electrode

through the electrolyte and separator to the negative electrode and the electrons migrate from positive electrode (aluminum current collector) via outer electrical connection to negative electrode (copper current collector).

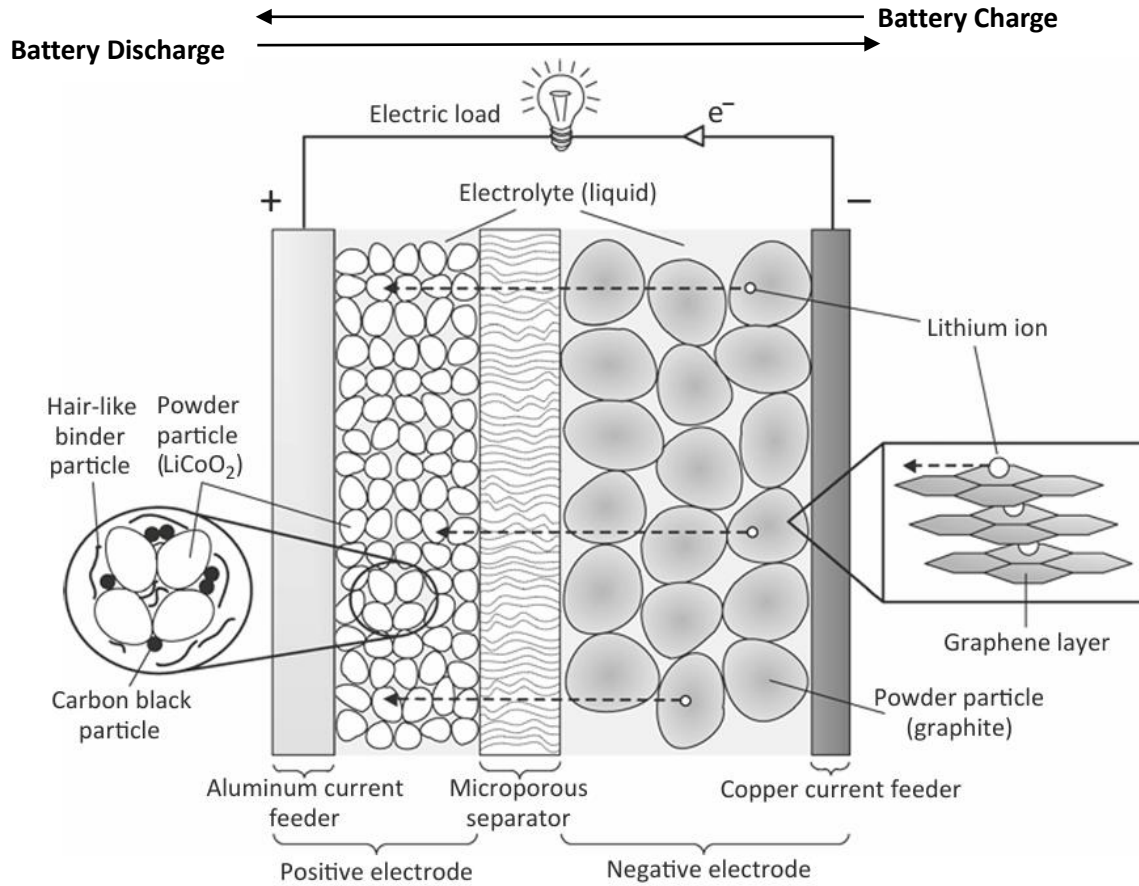


Figure 1-1: Components of traditional Li-ion battery during discharge

1.2.1 Cathode and Anode Materials for Li-ion Batteries

Lithium-ion batteries have revolutionized portable energy storage, generating voltages exceeding 3.5 V through the combination of cathode materials and carbonaceous anodes. The energy density of these batteries is a product of their voltage and capacity, with higher values in both aspects leading to superior performance. Inside a battery, the electrodes (mainly the cathode) are the limiting factors in terms of overall capacity, i.e. energy density, and cyclability which are primary determinants of the battery's overall energy output. The theoretical capacity of a material, expressed in mAh/g, represents the maximum charge it can

store and deliver based on its chemical composition, assuming complete utilization of all active material in the electrochemical reaction. In practice, however, not all lithium can be utilized without compromising the structural stability of the cathode material. This limitation gives rise to the concept of practical capacity, which refers to the actual usable capacity of the material in real-world applications. Practical capacity is the amount of lithium that can be safely extracted or stored during the battery's charge-discharge cycle without causing structural instability or degradation.

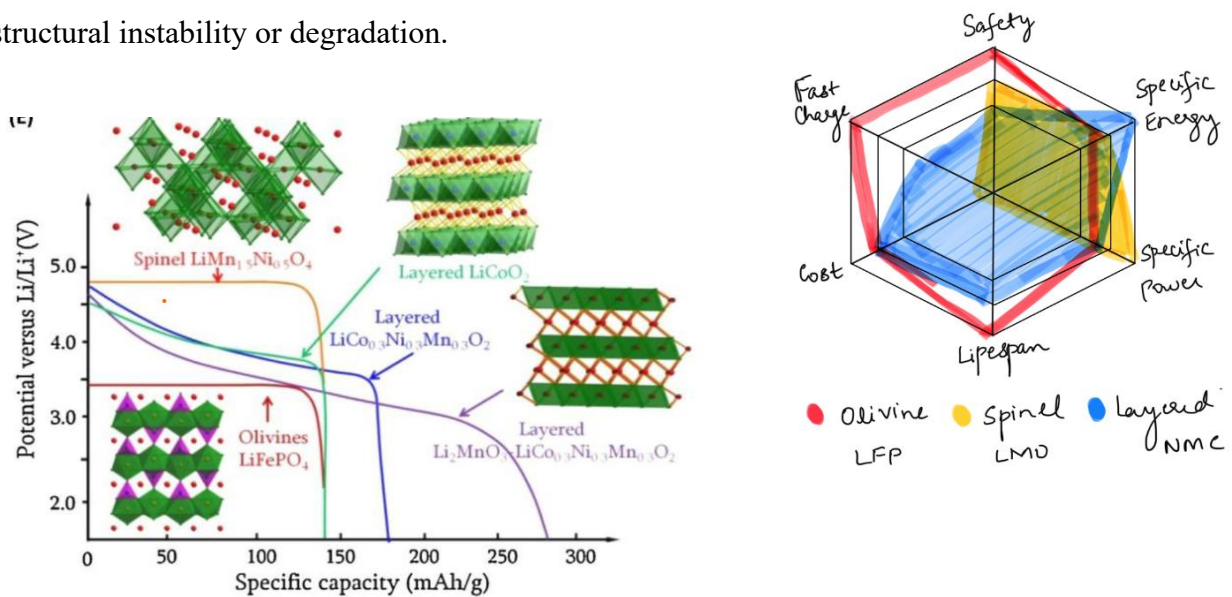


Figure 1-2: Classification of cathode materials used in Li-ion batteries [17][18][19]

Cathode materials for lithium-ion batteries are typically classified into three groups based on their crystal structure: layered oxides, spinels, and olivines as shown in Figure 1-2. Each structure offers distinct advantages and limitations. Layered oxides enable two-dimensional diffusion of lithium ions between metal octahedral layers, but often undergo phase transitions during cycling, resulting in sloping discharge curves. Spinel structures permit three-dimensional Li^+ diffusion, enhancing rate capability, but generally offer fewer available sites for lithium insertion and extraction, leading to lower specific capacities. Olivine structures, such as LiFePO_4 (LFP), feature one-dimensional channels for Li^+ movement, which can limit rate capability but often provides excellent structural stability. Every time Li is deintercalated

from the cathode structure a metal ion redox pair is formed M^{+n1}/M^{+n2} ($n_1 > n_2$) and this creates a potential of certain V vs Li/Li^+ which is the working potential of the cell. A flat discharge curve is ideal because it ensures a constant voltage output throughout the discharge cycle of battery (charging of the device), thus ensuring consistent power delivery.

Cathode Type	Material	Practical Specific capacity (mAh/g)	Operating Voltage (V)	Shape of discharge curve	Safety	Cost
Layered Cathode $LiMO_2$ M= Co, Ni, Mn, Al	LCO ($LiCoO_2$)	160	3.9	Flat	Fair	High
	NMC ($LiNi_{0.33}Mn_{0.33}Co_{0.33}O_2$)	200	3.7	sloping	Good	Low
	NCA ($LiNi_{0.8}Co_{0.15}Al_{0.05}O_2$)	200	3.7	sloping	Fair	Fair
Spinel LiM_2O_4 M= Mn, Ni	LMO ($LiMn_2O_4$)	100	4.1	flat	Good	Low
Olivine $LiMPO_4$ M=Fe, Mn, Co, Ni	LFP ($LiFePO_4$)	170	3.4	flat	Good	Low

Table 1-1: Properties of cathode materials used in Li-ion batteries [17][18]

Table 1-1 and Figure 1-2 compares commonly used positive electrode materials for Li-ion batteries. Layered oxides like NCM offer high capacity and working voltage but may pose safety risks due to potential oxygen evolution at high temperatures. Spinel structures like LMO provide good safety and low cost but at the expense of capacity. Lithium Iron Phosphite (LFP), an olivine structure, stands out for its exceptional safety profile, showing no thermal effects up to 300°C, and its stable, flat voltage discharge curve. While LFP may not boast the highest specific capacity or voltage among cathode materials, its combination of safety, environmental friendliness, and stable performance makes it an attractive option for many applications, particularly where safety is paramount.

Considering the various factors affecting cathode material performance, including capacity, voltage, safety, cost, and environmental impact, Lithium Iron Phosphate ($LiFePO_4$) has been selected as the cathode material for this project. Its outstanding safety characteristics and non-toxic nature make it particularly well-suited for wearable applications, where user safety and

environmental considerations are of utmost importance. While other cathode materials may offer higher energy densities, the balanced profile of LFP, combining good practical capacity, stable voltage output, and excellent safety features, positions it as an optimal choice for the development of reliable and safe wearable energy storage solutions.

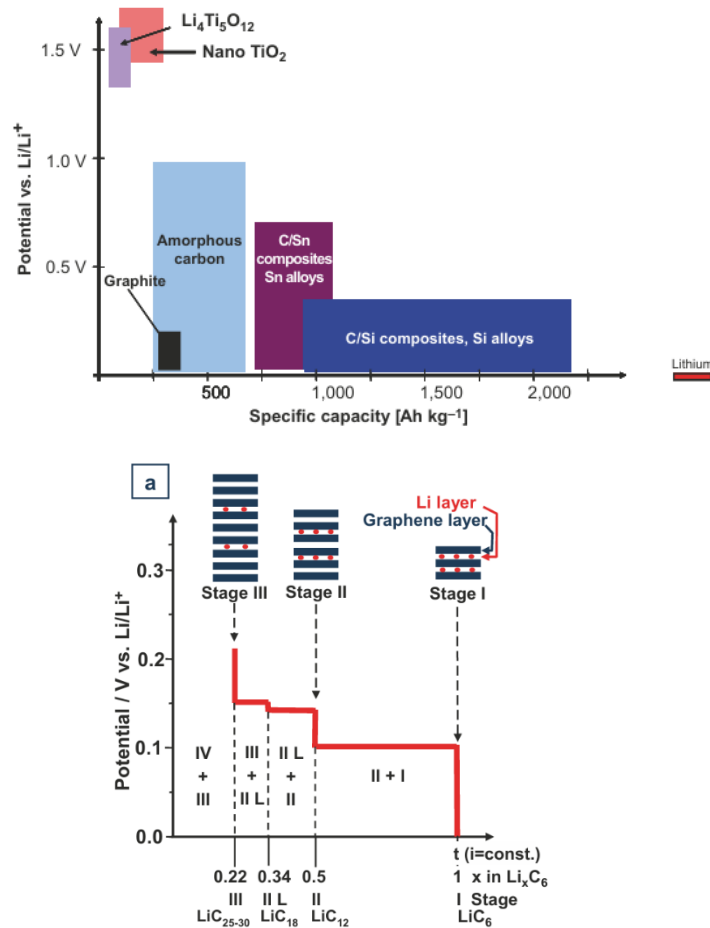


Figure 1-3: Classification of anode materials used in Li-ion batteries; (a) Stages of lithium intercalation into graphite at various voltages [18]

Secondary lithium cells initially employed metallic lithium foil as an anode, leveraging its impressive specific capacity of 3,860 mAh/g and very negative potential to achieve high cell voltages. However, this configuration presented significant challenges. The repeated dissolution and deposition of lithium during discharge and charge cycles led to decreased cycling efficiency. Moreover, lithium could form foam-like structures or dendrites during deposition, with the latter potentially growing through the separator. These dendrites posed

serious safety risks, potentially causing local short circuits that could result in complete self-discharge or, in extreme cases, trigger internal thermal chain reactions, fires, or explosions.

To mitigate these safety and efficiency concerns, researchers turned to lithium intercalation compounds as alternative anode materials. These compounds offer a balance of good capacity and high cell voltages while circumventing the risks associated with pure lithium anodes. The ideal anode material should possess high specific capacity and maintain a low potential versus lithium to maximize the overall cell voltage ($E_{\text{cell}} = E_{\text{cathode}} - E_{\text{anode}}$).

Table 1-2 shows various anode materials have been developed for different applications in Li-ion batteries, each with distinct characteristics. Graphite (Gr), a widely used anode material, exhibits well-defined two-phase plateaus during lithium intercalation, with specific chemical compounds forming at the beginning and end of each plateau as shown in Figure 1-3. The composition and the respective potential levels vs. lithium are as follows: $\text{LiC}_{36-50}/\text{LiC}_{25-30}$ (0.2 V); $\text{LiC}_{25-30}/\text{LiC}_{18}$ (0.1 V); $\text{LiC}_{18}/\text{LiC}_{12}$ (80-90 mV); $\text{LiC}_{12}/\text{Li}_6$ (65-85 mV)[20]. Its capacity is determined by the number of available graphene layers. Silicon anodes, while promising due to their high theoretical capacity, face challenges related to significant volume changes during lithiation, which can lead to the loss of well-defined insertion spaces and material amorphization over repeated cycles. Carbon/tin (C/Sn) alloy anodes encounter similar volume change issues and are further hampered by high manufacturing costs. Lithium titanate (LTO) stands out for its minimal particle volume change during cycling and very low cell impedance, resulting in excellent cycling stability and safety characteristics. However, LTO's advantages are offset by its very low electrical conductivity, low specific capacity, and high potential versus Li/Li^+ , which limits the cell's ability to operate at high voltages.

Among these options, graphite emerges as the most balanced choice, offering a favourable combination of performance and safety for many applications, including the targeted use of

Li-ion batteries in this context. Its stability, reasonable capacity, and well-understood behaviour makes it a reliable option for various energy storage needs.

Material	Practical Specific capacity (mAh/g)	Operating Voltage (V)	Safety	Volume expansion	Application
Graphite	360-380	0.01-0.25	Good	<1%	Portable electronic, Electric vehicles
Lithium Titanate LTO $\text{Li}_4\text{Ti}_5\text{O}_{12}$	160	1.55	Very safe	<10%	Grid energy storage Hybrid vehicles
Silicon alloys	1000-2300	0-0.4	Poor	High	Niche applications
C/Sn composite	993	0.05-1	Less	Very High 300-400%	Under research
Lithium	1840	0	Poor	Nil. Dendrite formation	Li-S Li-air batteries

Table 1-2: Properties of anode materials for Li-ion batteries.[18]

1.2.2 Solid Electrolyte Interface

An important feature for lithium graphite intercalation compounds in Li^+ containing electrolytes is the formation of solid electrolyte interface (SEI) film. During the first-cycle discharge of a cell as shown in Figure 1-4 (a), a part of lithium atoms transferred to the carbon electrode electrochemically will react with the nonaqueous solvent of the electrolyte, which contributes to the initial irreversible capacity. The reaction products form a Li^+ conducting and electronically insulating layer on the carbon surface called the SEI. This happens because the anode working voltage operating window is below the electrolyte decomposition voltage lower limit as shown in Figure 1-4 (b). But the SEI will not form in case of LTO anode as the operating voltage of LTO is always within the electrolyte stability window. Once SEI is formed, reversible Li^+ intercalation into carbon, through SEI film, may take place even if the carbon electrode potential is always lower than the electrolyte decomposition potential, whereas further electrolyte decomposition on the carbon electrode will be prevented.

The quality of the SEI greatly influences the cycling stability, service life, and safety of the Li-ion cells. Also, the thickness of the layer that the lithium ions in the electrolyte need to

migrate through increases. This increase causes a bigger mass transfer resistance which results in a higher electrical resistance.

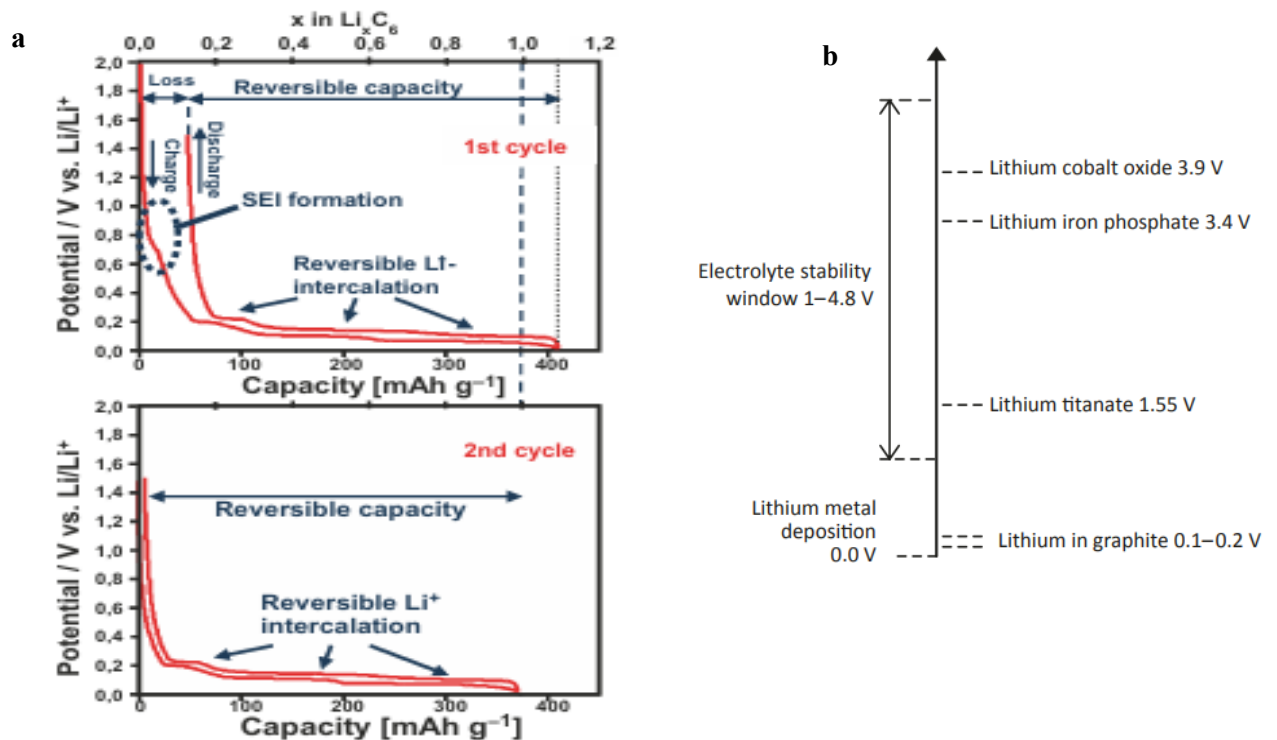


Figure 1-4: (a) Galvanostatic charging and discharging cycle of graphite with lithium metal as counter electrode and reference for the first (top) and second (bottom) cycle; (b) The potential range of electrolyte stability, compared to the potentials of common electrode materials [18][20]

The SEI is usually few Å in thickness consisting of an inner inorganic film containing Li₂O, LiF, Li₂CO₃ etc and an outer porous organic film consisting of polyolefins, semi carbonates etc. The inorganic film mainly produced by the decomposition of anions is thinner which provides mechanical stability to the SEI layer offers high conductivity for Li⁺ ions and prevents further electrolyte decomposition. The organic film formed by the decomposition products of solvent (organic electrolyte)/(cations of ionic liquid in case of ionic liquid electrolyte) provides elasticity to the SEI layer to accommodate the volume change during cycling. Anion derived SEI is superior as it decreases the activation energy for both Li⁺ desolvation and diffusion, facilitating faster ion transport and also hinders solvent co-intercalation, which would otherwise destroy the graphite lattice.

1.2.3 Battery Parameters and Electrochemical Cycling Test Procedure

Typical parameters used to characterize a battery cell or system are capacity, efficiency, capacity retention, electrical energy and power. Capacity, expressed in Ah describes the amount of electric charge a power source can deliver under specific discharge conditions. It depends on the discharging current, the cut-off voltage, temperature and type and amount of active material. Specific capacity (mAh/g) refers to the amount of electric charge a battery can store per unit of mass. Whereas the areal capacity (mAh/cm²) is the amount of electric charge a battery can store/provide per unit electrode area. The energy of a rechargeable battery is calculated as product of capacity and average discharge voltage. The specific energy refers to the energy per mass of the battery and its unit is Wh/kg. The efficiency is the energy released during discharging divided by the energy stored during charging in a given cycle. On the other hand, capacity retention is a measure of how much capacity a battery retains over time and cycles. It is calculated as percentage ratio of capacity of battery after a number of cycles by the initial capacity of the battery.

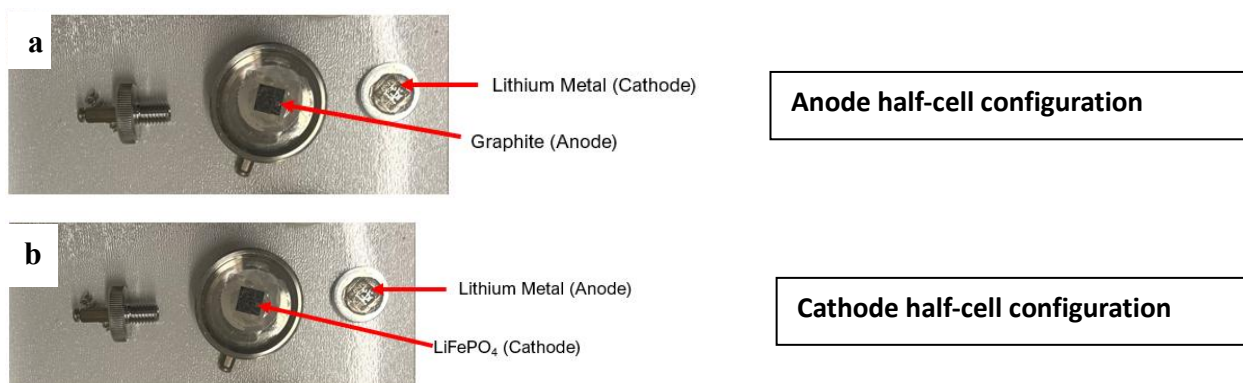
Another important battery testing parameter is the C-rate. It is the rate at which a battery can charge or discharge all of its energy (or power) relative to its maximum capacity. C-rate is described in relation to a 1h discharge, so 1C-rate is equal to the rate at which a battery is fully discharged (or charged) in 1h (Table 1-3). It is calculated as Current (mA) / Battery capacity (mAh) as shown in Table 1-3.

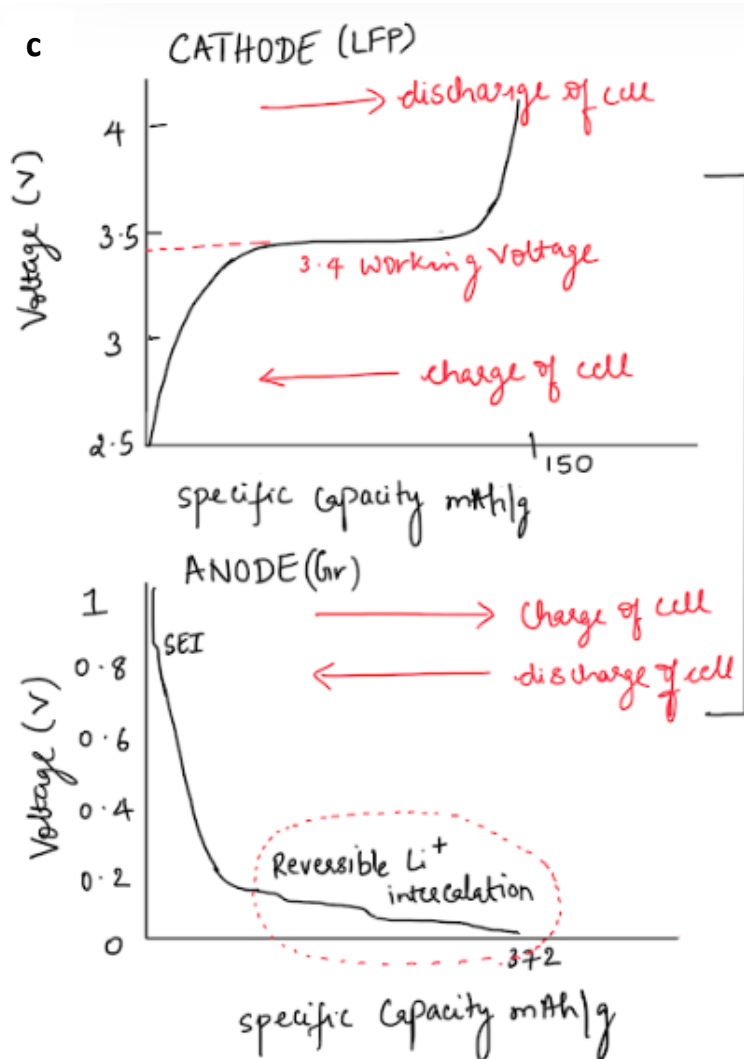
C-rate	Current (mA) assuming 1mAh capacity	Time taken (hr)
0.05	0.05	20
0.1	0.1	10
0.5	0.5	2
1	1	1
2	2	0.5
10	10	0.1

Table 1-3: Variation of charge/discharge current and time at various C rates.

The standard charging/discharging process followed for lithium-ion batteries in this work is the CC constant current method, where a constant current is maintained causing the ions to intercalate/deintercalate at the respective electrodes at a steady state. During the process the battery voltage increases/decreasing during the charge/discharge process until the cut-off voltage is reached. Depending on the materials used, Li-ion batteries can be charged and discharged at different determined maximum/minimum voltages but not any further. Overcharging the battery causes deterioration reactions that can damage the material structure and reduce the battery's lifespan. LiFePO_4 half-cell can be charged and discharged upto 4V and 2.5V respectively and Gr half cell can be charged and discharged upto 1.5V and 0.01V respectively as shown in Figure 1-5 (c). Therefore, we charge and discharge the LFP/Gr full cell upto 3.7V to 2.5V respectively. However, LTO anode can be charged and discharged upto 2.8V and 1V hence we charge and discharge the LFP/LTO full upto 2.5V and 1V.

Half-cell cycling is a process of repeatedly charging and discharging a single electrode in a cell configuration at various C rates where lithium metal serves as both the counter and reference electrode (Figure 1-5). This setup allows one to isolate and study the performance of a specific electrode material without the influence of a full battery's other components. As lithium metal provides an unlimited Li supply which helps us study the counter electrode materials performance like capacity, rate capability, cycling stability and material degradation mechanism and its compatibility with different electrolyte systems.





$$E_{\text{cell}} = E_{\text{cathode}} - E_{\text{anode}}$$

LFP/Gr charge/discharge limit= 2.5V – 3.7V

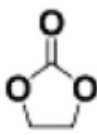
Figure 1-5: (a) Cathode half-cell configuration shown in a split cell; (b) Anode half-cell configuration shown in a split cell; (c) Cathode and anode half cycle charge/discharge curves.

1.3 Electrolyte Types Used in Li-ion Batteries

An electrolyte is a crucial component in a battery, serving as a medium for ion transport between the cathode and anode as shown in Figure 1-1. It must demonstrate stability against both electrode surfaces and undergo no net chemical changes during battery operation. All faradaic processes are expected to occur within the electrodes. An ideal electrolyte should meet several criteria: (1) It should be a good ionic conductor and electronic insulator, so that ion (Li^+) transport can be facile and self-discharge can be kept to a minimum; (2) It should

have a wide electrochemical window, so that electrolyte degradation would not occur within the range of the working potentials of both the cathode and the anode; (3) It should also be inert to other cell components such as cell separators, electrode substrates, and cell packaging materials; (4) It should be thermally stable, for liquid electrolytes both the melting and boiling points should be well outside the operation temperatures; (5) It must have low toxicity and successfully meet also other measures of limited environmental hazard; (6) It must be based on sustainable chemistries, meaning that the elements are abundant and the synthesis processes are as low impact as possible, and (7) it must carry as low total cost, materials and production, as possible.

Electrolytes for Li-based batteries can be classified into four main categories: non-aqueous electrolytes, ionic liquids (ILs), polymer electrolytes (including gel and solid polymer), and hybrid electrolytes. The most commonly used electrolyte is the non-aqueous electrolytes which consist of a lithium salt solubilized in an organic solvent or solvent mixture. Table 1-4 shows the characteristics of various solvents used to form non aqueous electrolytes. Table 1-5 describes the properties of most common lithium salts used in all the different electrolytes used in Li-ion batteries. While organic non-aqueous electrolytes offer lower viscosity and good ionic conductivity, they have poor thermal stability (low flash point) and are sensitive to moisture, are toxic in nature, which can be problematic in medical environments.

Solvent	Structure	Permittivity (25°C)	Viscosity mPa s (25°C)	Flash point °C
Ethylene carbonate (EC)		90	1.9	160

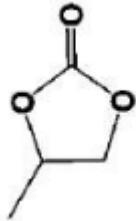
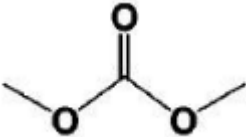
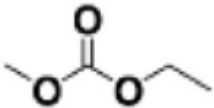
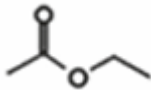
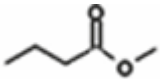

Propylene carbonate (PC)		65	2.5	135
Dimethyl carbonate (DMC)		3.1	0.59	15
Ethyl methyl carbonate (EMC)		3	0.65	23
Ethyl Acetate (EA)		6	0.45	- 4
Propylene acetate		5.6	0.60	11
Dimethyl ether (DME)		7.2	0.46	- 41

Table 1-4: Physico-chemical characteristics of battery solvents [18]

Polymer electrolytes play the role of both electrolyte and separator. In a standard polymer electrolyte, the lithium salt (charge carriers) are added to the polymer. Poly(ethyleneoxide) (PEO) is the common polymer used. The ether bridges of the polymer lattice provide for the conduction of lithium ions. In gel-polymer electrolyte a liquid electrolyte is incorporated within a polymer matrix (Poly (vinylidene fluoride) PVDF- commonly used). Here the ion transport is facilitated by both the polymer matrix and the incorporated liquid electrolyte. But the polymer electrolyte has lower ionic conductivity, narrow electrochemical window and low interfacial stability which increases the overall cell impedance in turn affecting the cycling performance of the cell.

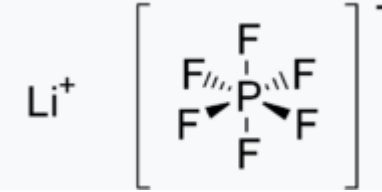
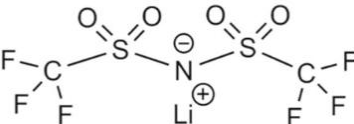
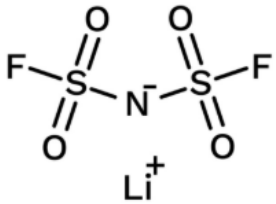
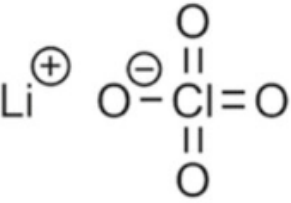

Salt	Structure	Comments
Lithium hexafluoride (LiPF ₆)		Highly conductive Electrochemically stable >4.8V vs Li/Li+ Thermally unstable Susceptible to hydrolysis
Lithium bis(trifluoromethanesulfonimide) LiTFSI		Highly conductive Electrochemically stable >4.8 vs Li/Li+ Hydrolysis resistant Thermally stable FSI anion is smaller in size than TFSI-, hence FSI- has lower viscosity
Lithium bis(fluoromethanesulfonimide) LIFSI		Expensive
Lithium perchlorate LiClO ₄		Strong oxidiser , safety concerns at high temperature Lower conductivity
Lithium bis(oxalate)borate LiBOB		Halogen free, environment friendly Thermally stable Electrochemically stable 4.5-5 V vs Li/Li+ Lower conductivity Susceptible to hydrolysis

Table 1-5: Physico-chemical properties of lithium salts used in electrolytes [18][21]

Ionic liquid electrolyte consists of a lithium salt (Li⁺X⁻) dissolved in ionic liquid (R⁺X⁻). They exhibit high ion conductivity, great chemical and electrochemical stability, large electrochemical stability window, low vapor pressure, and non-flammability. However, ILs have higher viscosities than organic liquids, which can result in reduced conductivities and mobility. But their properties can be tuned by various combinations of cation and anion used in the ionic liquid and the lithium salt.

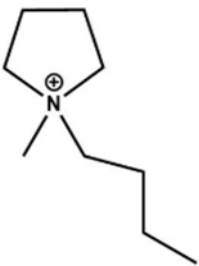
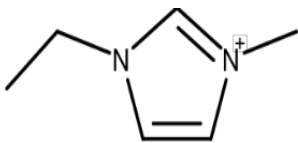
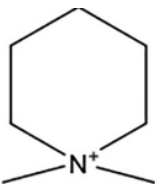
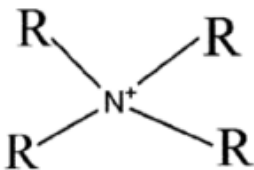
Cation Type	Structure	Comments
Pyrrolidinium	PYR ₁₄ cation N-Methyl-N-butyl pyrrolidinium 	<ul style="list-style-type: none"> SEI formation is better compared to other IL.
Imidazolium	EMIM cation 1-Ethyl-3-methylimidazolium 	<ul style="list-style-type: none"> charge delocalization leads to lower viscosity → higher ionic conductivity Better thermal stability among other IL SEI formation is problematic
Piperidinium		<ul style="list-style-type: none"> Larger in size than pyrrolidinium hence higher viscosity.
chain quaternary ammonium		<ul style="list-style-type: none"> aprotic nature → higher stability window up to 5V large molecular size → limited rotational freedom → lower ionic conductivity and viscosity Poor SEI in case of graphite anode → large capacity drop during cycling

Table 1-6: Classification of cations used in ionic liquids as part of the ionic liquid electrolyte [21]

Common cations used in ionic liquid electrolytes include imidazolium, quaternary ammonium, pyrrolidinium, and piperidinium as listed in Table 1-6, while common anions include PF₆⁻, TFSI⁻, and FSI⁻ as listed in Table 1-5. Based on their properties, PYR₁₄ (N-Methyl-N-butyl pyrrolidinium) and EMIM (1-Ethyl-3-methylimidazolium) cations show better ionic conductivity, lower viscosity, and stability among the options. The FSI⁻ anion offers advantages over TFSI⁻ in terms of viscosity, conductivity, anode compatibility, and

lithium-ion transport. For this study, LiFSI (salt): PYR₁₄FSI (ionic liquid) and LiFSI (salt): EmimFSI (ionic liquid) ionic liquid electrolytes are selected for li-ion battery fabrication, considering their favourable properties for wearable medical device applications.

1.4 Organization of This Work

The remainder of the thesis is structured as follows:

Chapter 2 introduces the concept of "battlet" and its fabrication approaches. It delves into a detailed comparison of surface topography and morphology differences between battlets fabricated using stencil printing and ink-jet printing methods. The chapter also discusses the importance of determining the optimal ratio of materials for electrode slurry composition. It analyses how variations in material ratios within the slurry affect the electrochemical performance of the battery.

Chapter 3 concentrates on electrolyte optimization for flexible lithium-ion batteries. It explores the selection of appropriate additives that aid in the formation of a stable Solid Electrolyte Interphase (SEI) on graphite surfaces when using ionic liquid electrolytes. The chapter further examines the process of selecting the most suitable ionic liquid electrolyte by varying factors such as molar ratio, viscosity, and cation/anion composition. The ultimate goal is to achieve electrochemical performance in flexible Li-ion batteries that is comparable to those using organic electrolytes.

Chapter 4 introduces an innovative approach to flexible battery design. It presents an interdigitated battlet design that alters the Li⁺ diffusion path, potentially overcoming the limitations of traditional battlet designs for flexible Li-ion batteries. The chapter demonstrates a fabrication approach for this new design, showcasing flexible current collectors on a PDMS substrate. It also describes the assembly and packaging of a flexible Li-ion battery with ionic

liquid electrolyte in a bent state. The chapter concludes by presenting the results of a preliminary electrochemical cycling study of the flexible interdigitated Li-ion battery.

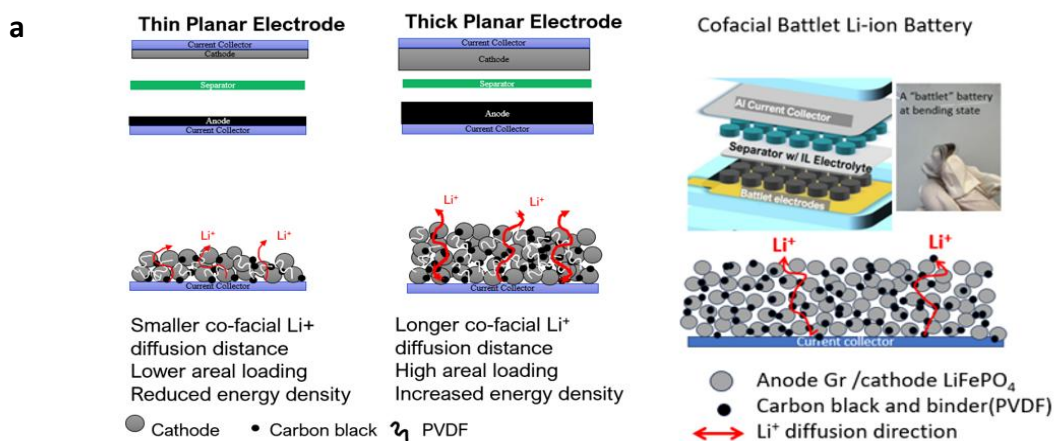
Chapter 5 provides a comprehensive summary of the findings of this thesis. It discusses potential future research directions and proposes further work based on the outcomes of the current research.

CHAPTER 2: FABRICATION OF THE BATTLET LI-ION BATTERY

In this chapter, the formulation of the electrode slurry to meet the specific areal capacity requirements of the electrode is presented. Following this analysis, advantages of ink-jet printing method over the screen-printing method is discussed. Detailed information on the morphology and mechanical performance of the electrodes is provided in this chapter.

2.1 Flexible Battlet Li-ion Battery Fabrication Process

To overcome the intrinsic issues of conventional batteries like limited flexibility, lack of biocompatibility, flammability etc we implement the dielet method in wearable electronics packaging to design and fabricate flexible Li-ion battery known as Battlet [22][23]. The battlet approach explodes a single large electrode into a small cell matrix and flexibly interconnects the cells via flexible current collector layers deposited on a flexible biocompatible substrate PDMS (poly-dimethyl siloxane) as shown in Figure 2-1. This battlet design can significantly reduce the stress concentration of the electrode during bending with conventional electrode materials. As the combined young's modulus of substrates (PDMS (2.1 MPa) + Parylene (2.8-5 GPa) + Al (70 GPa) or Cu (130 GPa)) is lower than the electrodes (LFP/Gr + PVDF + CB) the bending occurs between the battlet electrodes thus reducing the stress on the electrode as shown in Figure 2-1(c) [23].



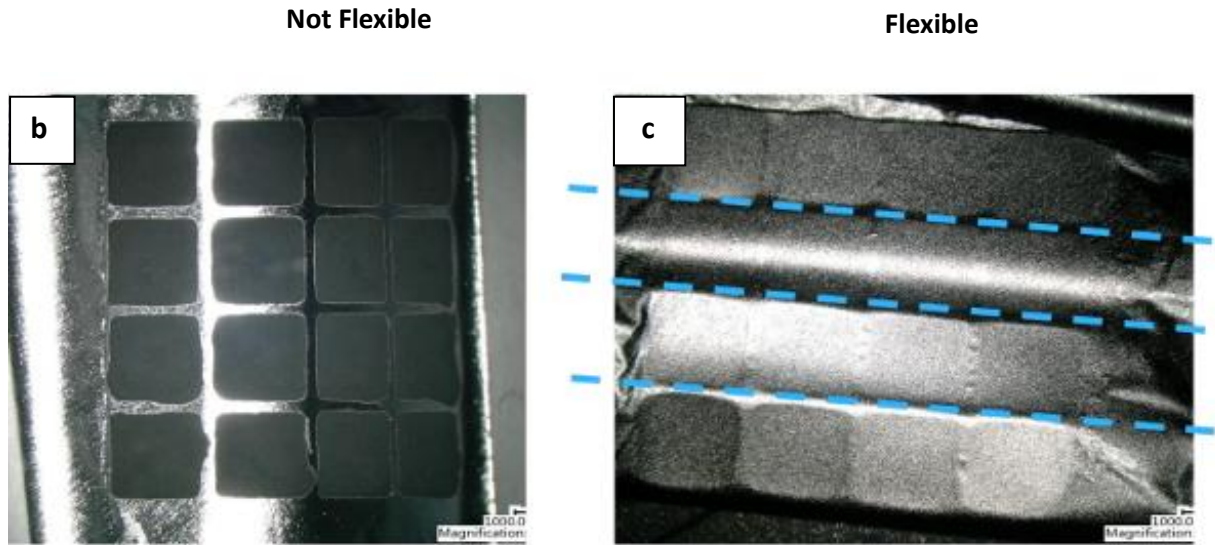


Figure 2-1: (a) Comparison of the conventional planar structure and the Battlet structure; (b) battlet electrode before bending; (c) Battlet electrode after bending [23]

2.1.1 Packaging of Battlet Li-ion Battery

Figure 2-1(a) shows the exploded view of the battlet battery structure. The top and bottom PDMS is as a sealing and substrate. The cathode battlet and anode battlet are aligned and separated by a separator of 25 μm thickness. In addition, a double side polyimide tape ring is placed on the edge of the electrode as an electrolyte reservoir. Ionic liquid with additive is used as battery electrolyte. Figure 2-2 shows the fabrication process of the full battlet battery. Initially, a double-sided thermal release tape is laminated onto a 4-inch glass wafer. Then, uncured PDMS is spin-coated at 2000 rpm on the substrate and cured at room temperature. The PDMS coating is typically less than 100 μm thick. A 2 μm Parylene C layer is deposited on the PDMS via chemical vapor deposition as a buffer layer to mitigate the CTE mismatch of PDMS and current collectors. Subsequently, 600 nm of Al is sputtered on the Parylene layer as the cathode current collector. The sheet resistivity is 4 $\mu\Omega\cdot\text{cm}$ in evaporation of Al film. Simultaneously, a 20/600 nm Ti/Cu film is sputtered on another substrate as the anode current collector. Next the battery materials are deposited onto the flexible current collectors. After that, the electrode slurry is vacuum dried at 100 $^{\circ}\text{C}$, and a double-sided polyimide ring

is applied at the cathode and anode edges as a seal and electrolyte reservoir. The separator is then placed on the electrode, and the ionic liquid electrolyte with an additive is added. Ionic liquids are novel liquid materials composed only of anions and cations with unique properties such as very low saturated vapor pressure [14], good ionic conductivity [15], good thermal stability [16], non-flammability, and wide electrochemical window. These properties not only create new opportunities for the design of new Li-ion battery materials with higher energy/power density, better long-cycle stability, and safety, but also offer new possibilities for innovation with new type of battery forms, especially for wearable devices. Finally, the battery cathode and anode are sealed with double-sided polyimide tape, completing the flexible battlet batteries after releasing the PDMS from the wafer handler.

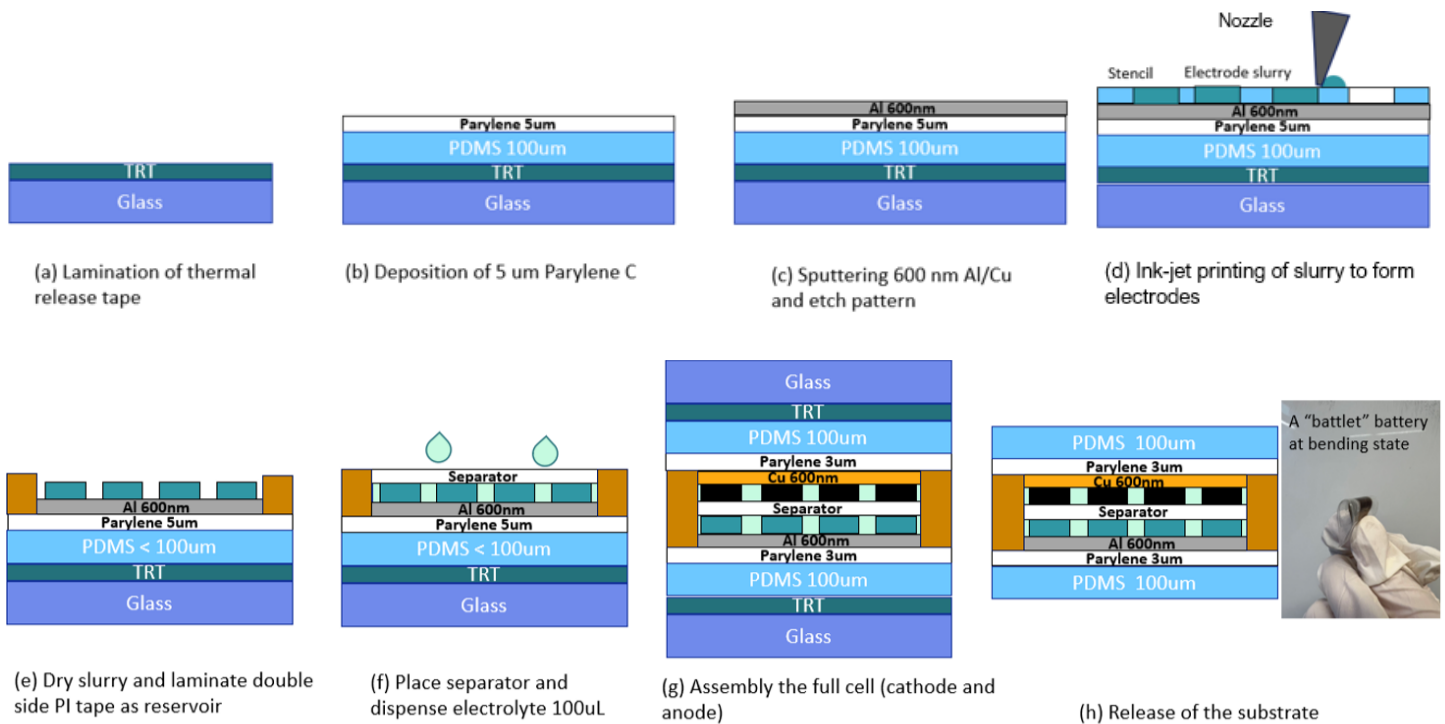


Figure 2-2: Fabrication process of the battlet flexible Li-ion battery

2.1.1 Fabrication of the Battlet Electrode

The following materials were used for the preparation of the slurry in this work: Lithium Iron Phosphate (LiFePO_4 , LFP, MSE Supplies) as cathode, Poly-vinylidene fluoride (PVDF,

Sigma-Aldrich) as binder, Super P carbon black (CB, MSE Supplies) as conductive agent and Graphite (Gr, MSE Supplies) or Lithium Titanate ($\text{Li}_4\text{Ti}_5\text{O}_{12}$, LTO, MSE Supplies- Chapter 4) as anode. The binder PVDF is needed to ensure good cohesion of the electrode particles and sufficient adhesion to the current collector. PVDF forms hair-like structures that efficiently keep the coating together as shown in Figure 2-3. As PVDF is not soluble in water, N-methyl pyrrolidone (NMP, Sigma Aldrich) is used as the solvent. It is vaporized during the drying of the composite electrode, and thus the finished cell does not contain any NMP. Carbon black is used as conducting additive. The amount of PVDF and carbon black should be just enough to ensure good contact and conductivity. As the additives do not contribute to the overall capacity, adding large amounts is not favourable. LiFePO_4 / Gr : PVDF : CB are mixed in an optimised ratio (to be discussed) and stirred for 24hrs to form a uniform cathode and anode slurry.

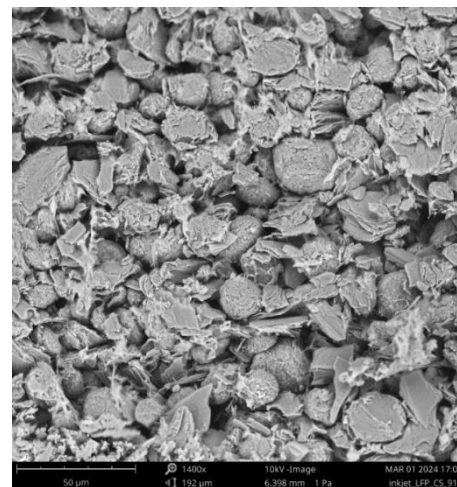
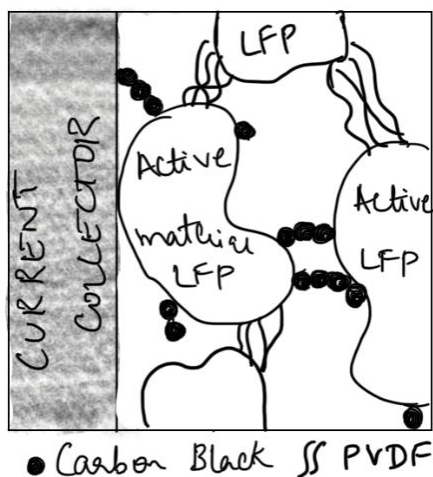


Figure 2-3: Interactions of materials in the electrodes (left); SEM image at 1400x of cathode electrode showing the LFP particles being held together by PVDF particles.

Two approaches were tested to dispense the slurry onto the current collectors to form the battlet electrode structure. 1. Stencil Printing and 2. Ink-Jet Printing. In the stencil printing process, the slurry is dispensed with a stencil on Aluminum (16µm) (cathode) or Copper

(16 μ m) (anode) current collectors to form the battlet design electrodes as shown in figure 2-4. In the latter process we use an Ink-jet printer (Voltera Nova) to dispense the slurry onto the current collector. The printer uses a direct-write technology to extrude materials and creates the desired pattern on the substrate as shown in figure 2-4 (b)(c). The printed electrodes are then dried in vacuum oven at room temperature for 24hrs. The thickness or the weight of the material deposited can be varied by varying the stencil material thickness or linearly increasing the print height or print pressure during ink-jet printing. Here we use a 100 μ m thickness stencil made from PDMS (sticky side)/parylene (top handling side).

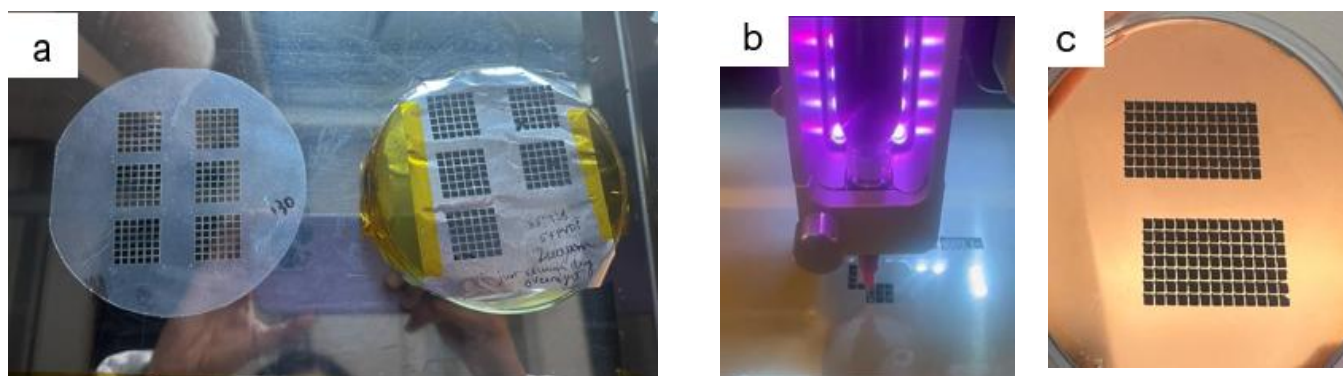


Figure 2-4: (a)Stencil Printing method (b) Ink-jet printing method (c) Printer electrode on flexible current collector

Figure 2-6 (a) and (b) shows the cathode and anode optical images printed using stencil and inkjet printer, respectively. Each cathode cell is 2.4 x 2.4 mm with 0.5 mm spacing, and each anode cell is 2.5 x 2.5 mm with 0.4 mm spacing. Anode cells are 0.1 mm wider than cathode cells to prevent the deposition of lithium and formation of lithium dendrites on anode surface during charging which can lead to short circuit. The weight of the anode and cathode are decided in such a way that the ratio of capacity of anode (negative electrode)/capacity of cathode (positive electrode) generally called the N/P ratio is between 1.2-1.3. This ensures that the anode has sufficient capacity to intercalate all available Li^+ ions from the cathode

during charging. The N/P ratio can also be controlled by making the anode larger in area rather than making changes in the thickness of the electrode as shown in Figure 2-5

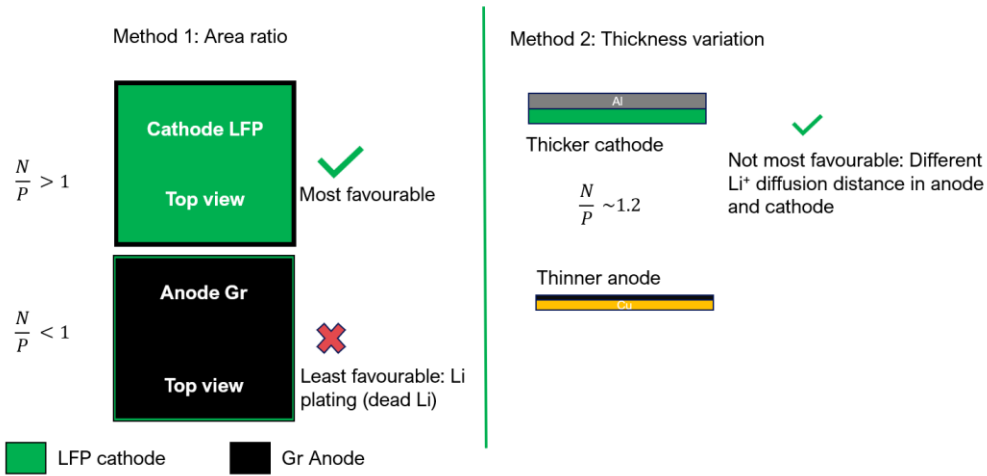


Figure 2-5: Methods to maintain optimal N/P ratio in LFP/Gr cell.

Figure 2-6 (c) presents the cathode cells surface profile and height map, with an average thickness of 30-40 μm and a capacity loading of about 1 mAh/cm^2 , equivalent to 5.88 mg/cm^2 of LFP. The cross-section indicates that the cell edges are about 5-10 μm higher than the center due to the stencil printing process. The anode's average thickness is about 20 μm , with a weight loading of about 1.5 mAh/cm^2 , equal to 4.2 mg/cm^2 . This difference in weight loading of anode and cathode is because the theoretical capacity of LiFePO_4 and graphite is 170 mAh/g and 372 mAh/g respectively. Maintaining the N/P ratio of 1.2 with just changing area ratio of cathode/anode resulted in a large area difference for anode and cathode which is not feasible for flexibility after alignment. Hence a combination of area ratio and thickness ratio variation was adopted as shown in Figure 2-5. Anode is printed at lower weight loading to maintain the N/P ratio of the full cell within 1.2-1.3. The screen-printing approach results in a concave shape of the battlet electrode due to the surface tension of the slurry and the stencil's properties. Consequently, both cathode and anode exhibit thickness variations within each battlet. This difference in thickness can increase electrode polarization during cycling

and cause nonuniform lithiation in the electrode materials during operation, thus reducing the battery's cycling life. Figure 2-6(d) also shows the cathode cells surface profile and height map with an average thickness of 50 μm and a capacity loading of about 1.3mAh/cm² equivalent to 7.6 mg/cm² of LFP. This shows a reduction in surface roughness from 10.15 μm to 3.56 μm . Additionally, weight loading variation decreased from 15.6% to 4.5%.

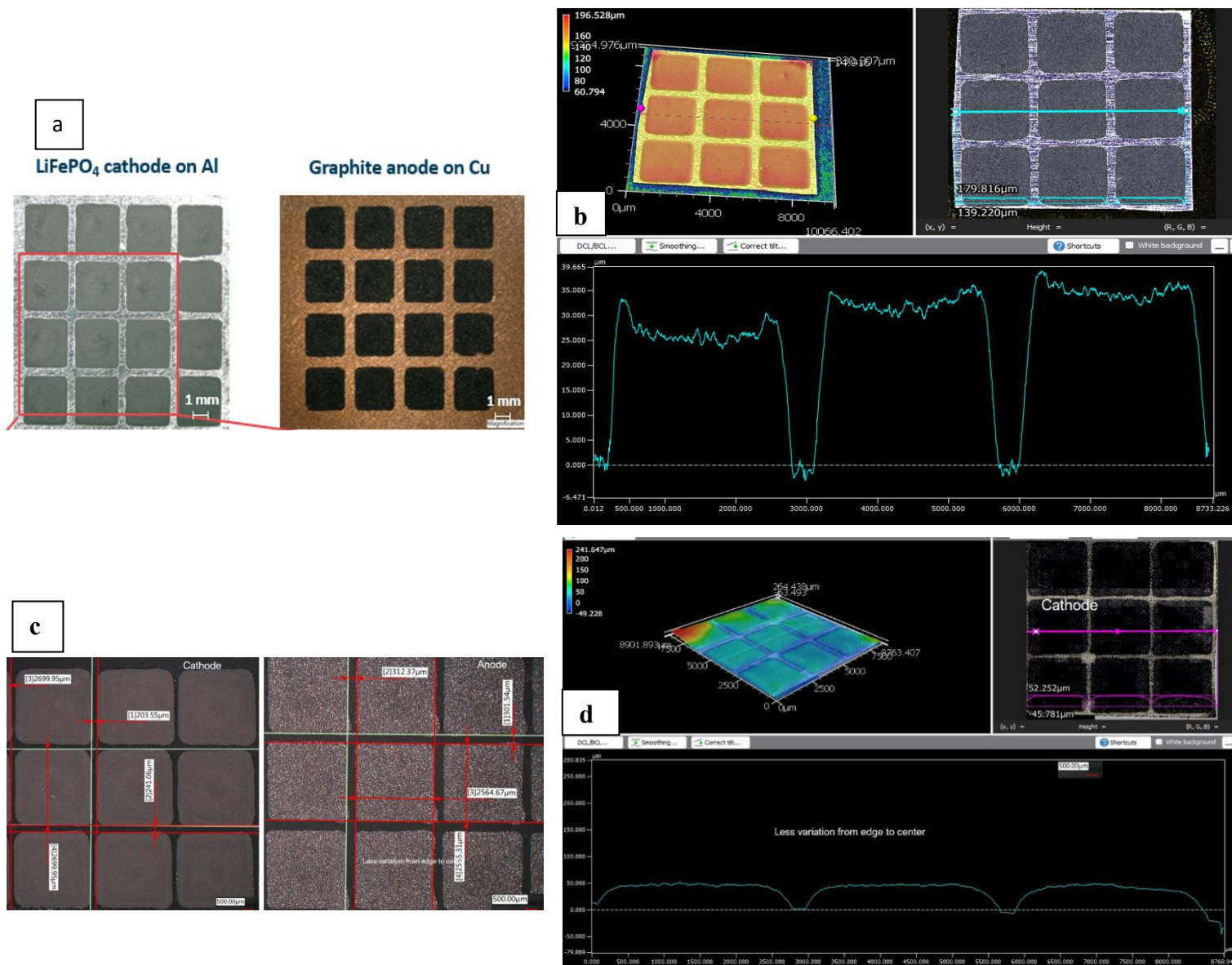


Figure 2-6: Optical images of cathode and anode battlet using (a) Stencil printing (b) Ink-jet printer; Confocal microscope images of the surface profile of cathode electrode using (c) stencil printing and (d) Ink-jet printer.

These results suggest that the inkjet approach offers better slurry distribution than screen printing, and an improvement from a concave to a more uniform, battlet profile. The ink jet printing also ensures good repeatability and can cover larger printing area in one stretch of printing cycle when compared the stencil, which is limited by the size of the stencil.

Figure 2-7 provides a detailed illustration of the surface characteristics of cathode and anode battery electrodes after printing and drying processes. The cathode, composed of LFP (Lithium Iron Phosphate) particles with a D90 of less than 1 μm , exhibits a smoother surface with higher porosity. The surface appears uniform and smooth, with distinct separations at the corners, indicating well-segmented and non-interconnected cells.

For the anode, as depicted in Figure 2-7(c) and (d), the corners are also clearly defined, demonstrating well-segmented cells. The graphite powder used in the anode has a significantly larger particle size, ranging from 20-30 μm , compared to the LFP particles. The graphite grains appear intact without any visible cracks. A notable feature of the anode surface is the network-like mesh structure, attributed to the PVDF binder material.

Precise measurements reveal that the average LFP particle size is 1.12 μm with a porosity of 51.688%, while the average graphite particle size is 30 μm with a porosity of 35.68%. This porous structure is crucial for effective electrolyte wetting of particles at all depths and ensures unimpeded diffusion of Li^+ ions throughout the electrode thickness. The observed morphological differences between the cathode and anode surfaces are primarily due to the disparate particle sizes of LFP and graphite. The smaller LFP particles contribute to a smoother, more uniform cathode surface, while the larger graphite particles result in a more textured anode surface. These structural characteristics play a significant role in the electrochemical performance and flexibility of the battery electrodes.

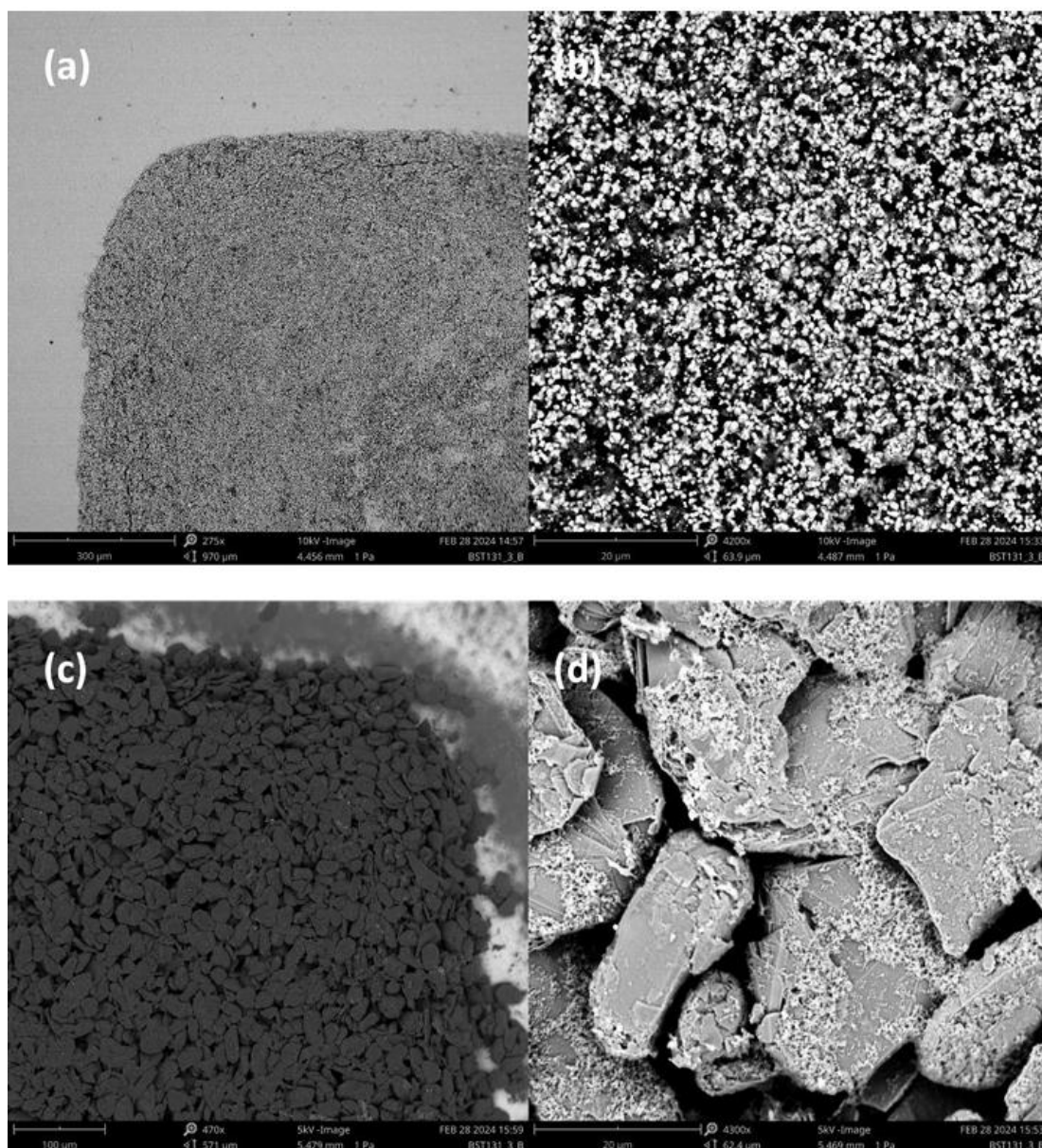


Figure 2-7: SEM images of (a) cathode battlet surface at corner (b) zoom on image of cathode at 4000x (c) anode battlet surface at corner (d) zoom in image of anode at 4000x

2.2 Optimization of Electrode Slurry Composition and Thickness

The theoretical capacity of graphite (372 mAh/g) significantly exceeds that of LFP (170 mAh/g). In a battery, the overall capacity is limited by the material with the lowest theoretical capacity, which in this case is the cathode material LFP. To address this limitation, three potential approaches are considered:

1. Alternate cathode materials: Switching to materials like Lithium Cobalt Oxide (LCO, 274 mAh/g) or Lithium Nickel Cobalt Manganese Oxide (NCM, 275 mAh/g) could increase cathode capacity while maintaining lower cell thickness. However, this option is not pursued due to the selection of LFP for its safety advantages and absence of harmful heavy metals, making it suitable for wearable device applications.
2. Enhancing electrode coating thickness: Increasing the coating thickness could lead to higher capacity but may result in increased ionic and electronic impedance due to longer diffusion paths for ions and electrons as shown in Figure 2-8.

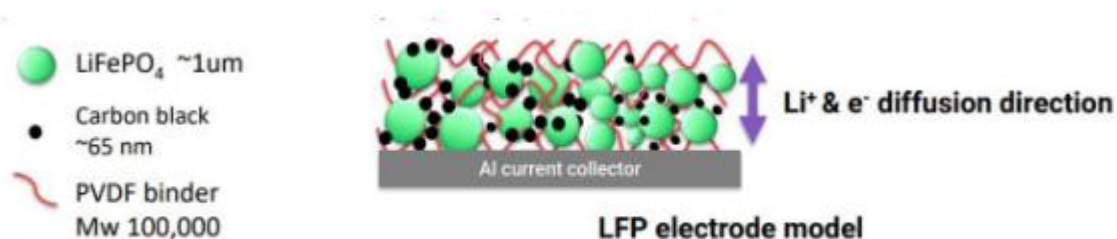


Figure 2-8: Structure model of LFP electrode [23]

3. Increasing LFP percentage in slurry: This approach could improve cathode capacity but may lead to higher film resistance due to reduced carbon black content and lower electrode-to-current collector adhesion strength from reduced PVDF content.

Sample ID	LFP: CB: PVDF weight ratio	Coating thickness(μm)	LFP loading density (mg/cm^2)
811-1	8:1:1	100	5.5
811-2	8:1:1	200	8.11
8587-1	8.5:0.8:0.7	100	6.46
8587-2	8.5:0.8:0.7	200	7.99
8515-1	8.5:1:0.5	100	8.5
8515-2	8.5:1:0.5	200	9.69
955-1	9:0.5:0.5	100	10.34
955-2	9:0.5:0.5	200	13.1

Table 2-1: Design of experiment for optimization of electrode slurry

To optimize these trade-offs, eight different composition ratios and coating thicknesses for LFP cathodes were examined as shown in Table 2-1. The LFP:Carbon:PVDF ratios ranged from 8:1:1 to 9:0.5:0.5. The coating thickness is the thickness of the stencil and not the final thickness after drying the electrodes. Figure 2-9 and Figure 2-10 show the key parameters including electrode thickness, loading density, theoretical capacity, and final area capacity that were measured for each sample. The study revealed that electrode thickness becomes a significant factor when exceeding 60 μm , with most samples achieving about 90% of their theoretical capacity. Most samples demonstrated a measured capacity of approximately 90% of the theoretical value. However, a decline in capacity was observed for the 955-1/2 samples, which was attributable to their increased thickness and sub-optimal quality. Notably, commercial LFP electrodes typically exhibit capacities between 1-1.5 mAh/cm². The optimal coating thickness and composition were determined to be 8.5:0.8:0.7 at 60-70 μm , achieving 1-1.2 mAh/cm², which is comparable to commercial LFP electrodes.

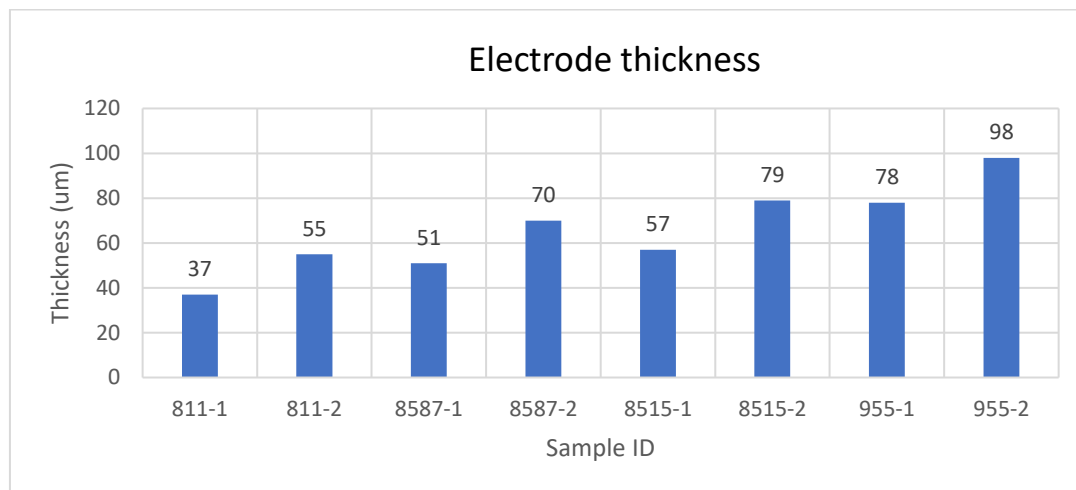


Figure 2-9: Variation of electrode thickness with different slurry composition and stencil thickness

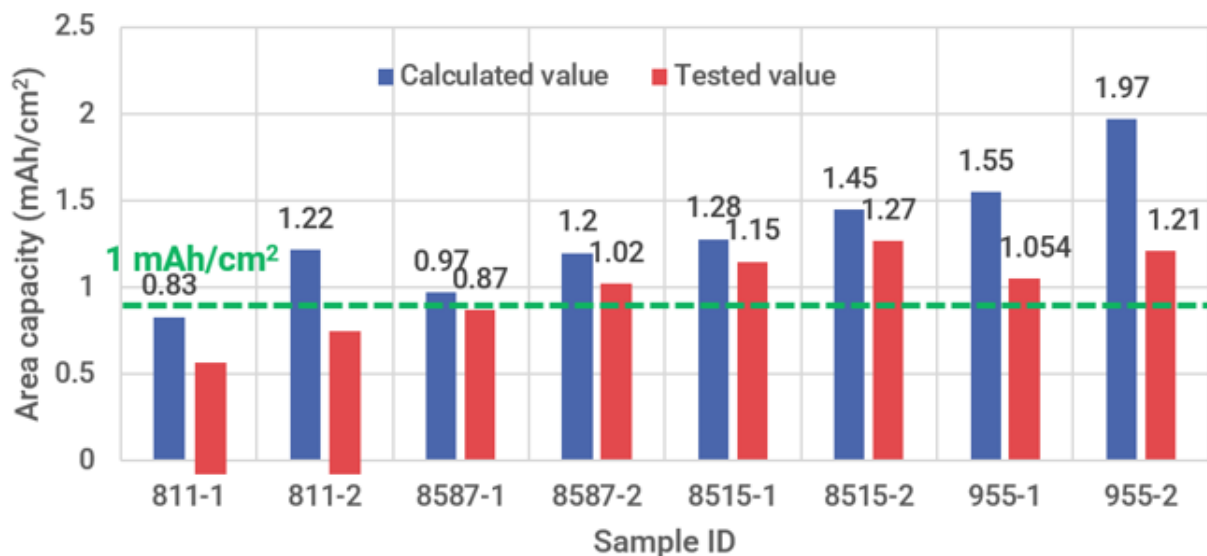


Figure 2-10: Comparison of theoretical and tested electrode capacity at different electrode composition and thickness.

Further analysis of film coating thickness and composition ratio showed that at 100 μm , the film remains intact without cracks. However, increasing thickness to 200 μm results in crack formation in the dry electrode due to internal stress during drying as shown in Figure 2-11. The actual electrode thickness after drying is typically 30-40 μm for a 100 μm thick stencil and proportionally thicker for a 200 μm stencil.

To solve cracking in thicker electrodes, ink-jet printing was used. This deposits slurry layer-by-layer, creating uncracked, thicker electrodes. Figure 2-6 (b) and (d) shows a thicker 50 μm electrode printed using ink-jet printer without any cracks. It handles thicker slurries for greater material deposition and uniform distribution, unlike stencil methods. Ink-jet printing offers fine control over electrode properties, advancing flexible, high-performance batteries for wearables.

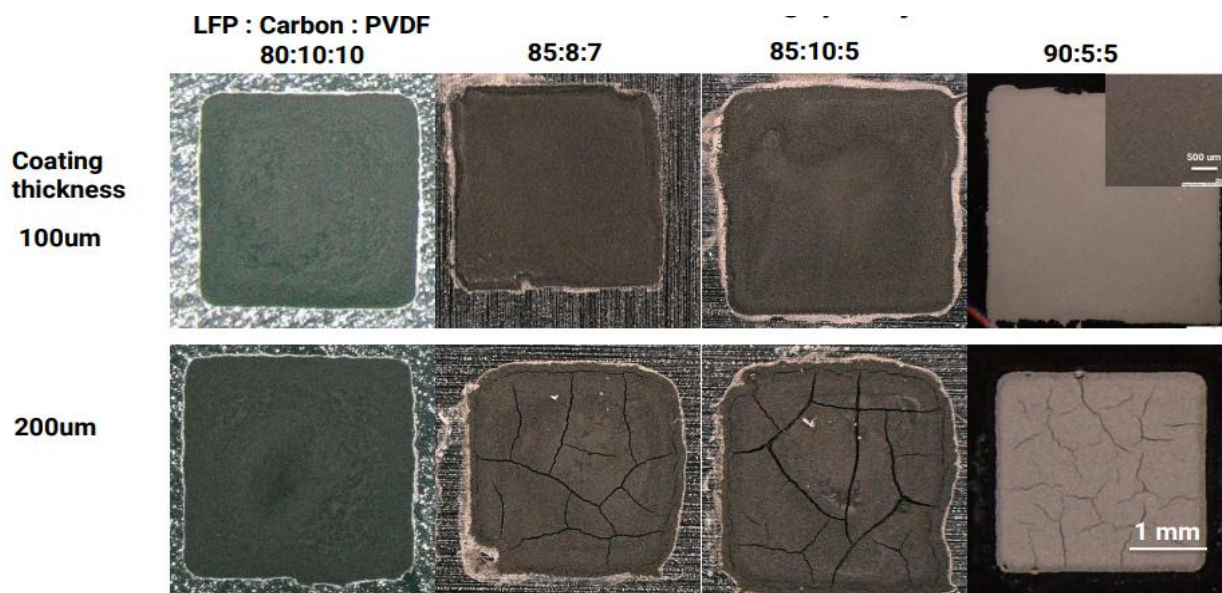


Figure 2-11: Optical images of dried LFP electrode surface fabricated using different slurry compositions and stencil thickness.

2.2.1 Electrode Preparation for Electrochemical Testing

Based on the slurry optimization study in the previous section a cathode slurry consisting of 85 wt.-% LFP, 8 wt.-% CB, and 7 wt.-% PVDF is prepared. Anode slurry consisting of Graphite: CB: PVDF in 91:5:4 ratio is prepared and both the slurries are stirred for 24hrs. The slurry was printed in the form of a 9x9 battlet cell array on aluminum (cathode)/ Copper (anode) foils and dried overnight under reduced pressure. The obtained electrodes were then manually cut into 3x3 battlet cell sizes and dried under vacuum at 100°C. Next, the electrodes were assembled in Swagelok cells (MTI Corporation) for initial study and also on FlexTrate™ platform (flexible package) in the Glove Box (MTI Corp) for electrochemical cycling study. 25μm monolayer microporous membrane (PP), surfactant coated (Celgard) was used as a separator. The electrolytes used in this study are as follows 1M LiPF₆ in DMC: EC (1:1vol, Solvionic), 1M LiPF₆ in FEC:DMC (2:8 vol, Dunn Lab) LiFSI: EmimFSI (1:9 mol ratio, Solvionic), LiFSI: PYR₁₄ FSI (1:9 mol, Solvionic), LiFSI: PYR₁₄FSI (2:3 mol,

prepared by adding LiFSI salt to LiFSI: PYR₁₄ FSI 1:9 electrolyte) and), LiFSI: EmimFSI (2:3 mol, prepared by adding LiFSI salt to LiFSI: EmimFSI 1:9 electrolyte). Vinylene Carbonate (VC, Sigma-Aldrich) and Fluroethylene carbonate (FEC, Sigma-Aldrich) is used as additive. Due to the manual cutting of 3x3 electrodes and weight calculation based on a 3x3 blank foil sample, there is a $\pm 10\%$ deviation in the actual electrode weight. This deviation can result in some cycling curves showing higher specific capacity values than the theoretical specific capacity, particularly when there is a negative deviation in the actual weight.

CHAPTER 3: ELECTROCHEMICAL STUDY

3.1 Selection of Electrolyte Additive for Optimal Anode Cycling Performance in Ionic Liquid Electrolyte

The electrolyte comprises of 3 classes of materials, 1. Conducting Salt, 2. Solvent, and 3. additives. It is the combination of these components that largely determines the physico-chemical and electrochemical characteristics of electrolyte. The role of the solvent is to dissolve lithium salt (high solvation) in a sufficiently high concentration while maintaining lower viscosity and electrochemical stability over an operating voltage (up to 4V) and temperature range. On the other hand, the main function of the salt is to exhibit maximum solubility in the solvent and completely dissociate in the solvent to ensure high Li ion mobility between the electrodes during charge/discharge cycles. It should also have a strong electron-withdrawing group to minimize the anion cation interactions and prevent the corrosion of aluminum current collector at potential above 3V vs Li/Li⁺. The selection of an ionic liquid electrolyte for this work has been discussed in Chapter 1.

During the initial stages of charging a Li-ion battery a solid electrolyte interphase SEI is generated on the graphite surface. This layer acts as a passivation layer to inhibit further electrolyte reduction. To improve the stability of this SEI film and increase first cycle efficiency additives are added to the electrolyte. Unsaturated ester additives such as vinylene carbonate (VC), vinyl ethylene carbonate (VEC), fluoroethylene carbonate (FEC) are common additives used to produce a good SEI film on the anode to improve initial coulombic efficiency and cycling performance as shown in Figure 3-1.

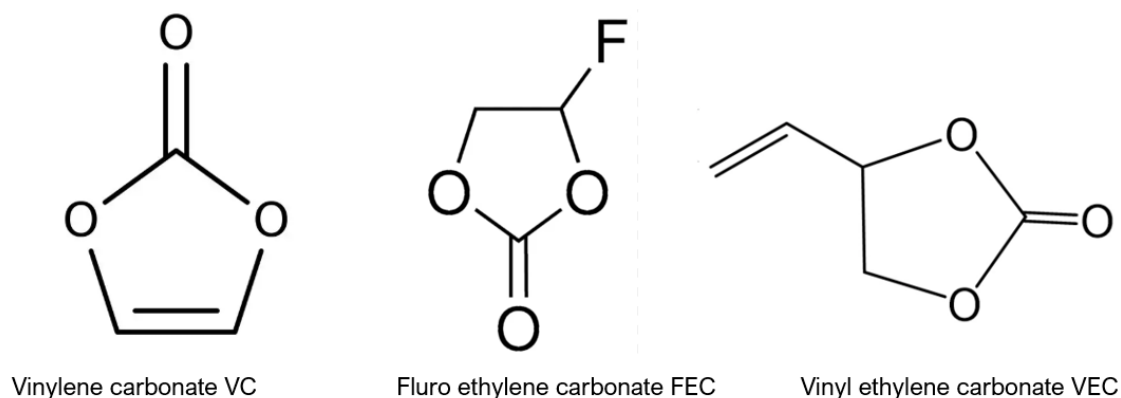


Figure 3-1: Additives used in Li-ion batteries

Decomposition of one VC molecule at anode consumes one lithium and one electron resulting in poly (VC) as the main reaction product and small quantities of HCO_2Li , $\text{Li}_2\text{C}_2\text{O}_4$ to form a purely organic SEI. The relatively high VC consumption and low lithium ion per reduced VC molecule consumption results in a thick and Li-poor SEI film. On the other hand one molecule of FEC decomposition consumes 3 Li^+ plus 3 electrons, yielding an SEI composed of mainly LiF and other products like Li_2CO_3 , $\text{Li}_2\text{C}_2\text{O}_4$, HCO_2Li and poly(VC) units resulting in an inorganic rich SEI film. The addition of FEC promotes the formation of LiF-rich and dense SEI film which leads to uniform Li deposition and inhibits the formation of disordered Li dendrites [24][25]. It has also been shown that Li^+ has lower diffusion barrier in LiF decorated interface[25].

As the additive greatly influences the anode performance, we carried out an electrochemical study of graphite half-cell in 1M LiPF_6 in FEC: DMC (2:8 vol) and 1M LiPF_6 in EC:DMC (1:1 vol) + 5%VC (Figure 3-2) to study which additive would be suitable for the testing of our flexible battlet full cell. We also studied the effect of these additives in the case of an ionic liquid electrolyte by testing anode half-cell in $\text{LiFSI}:\text{PYR}_{14}\text{FSI}$ (2:3) + 5%VC and $\text{LiFSI}:\text{PYR}_{14}\text{FSI}$ (2:3) + 5%FEC ionic liquid electrolyte (Figure 3-3). The cathode, anode,

and electrolyte in anode half-cell during discharge are Li metal (0.6 cm^2) (circle of radius 0.43 cm), Graphite ($3 \times 3 \text{ cell } 0.5 \text{ cm}^2$), and $1 \text{ M LiFSI PYR}_{14}\text{FSI } 2:3$ ($100 \text{ } \mu\text{L}$). The loading density of battlet electrodes in case of organic electrolyte and ionic liquid electrolyte is 5.64 mg/cm^2 and 6.18 mg/cm^2 respectively which provides an areal capacity of 2 mAh/cm^2 and 2.3 mAh/cm^2 respectively. The thickness of the anode battlet for this loading was $\sim 25 \mu\text{m}$.

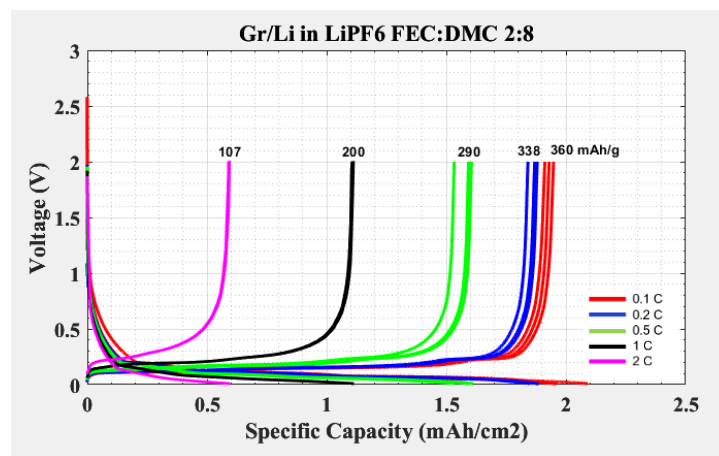
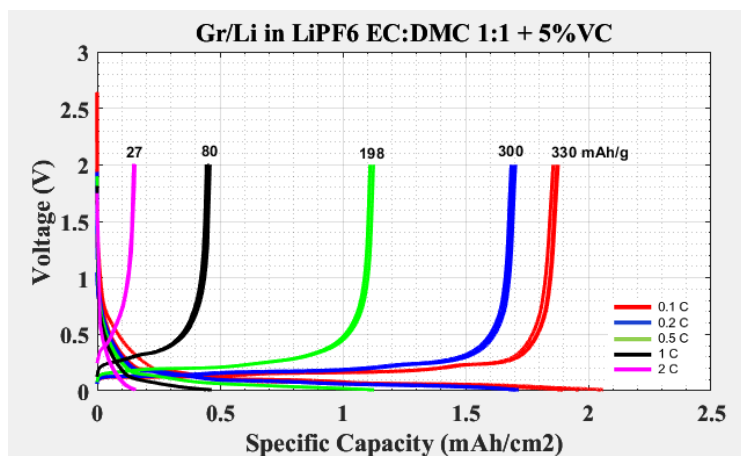


Figure 3-2: Charge/Discharge cycling at different C rate of anode half cells in organic electrolyte with (a) VC additive (b) FEC additive.

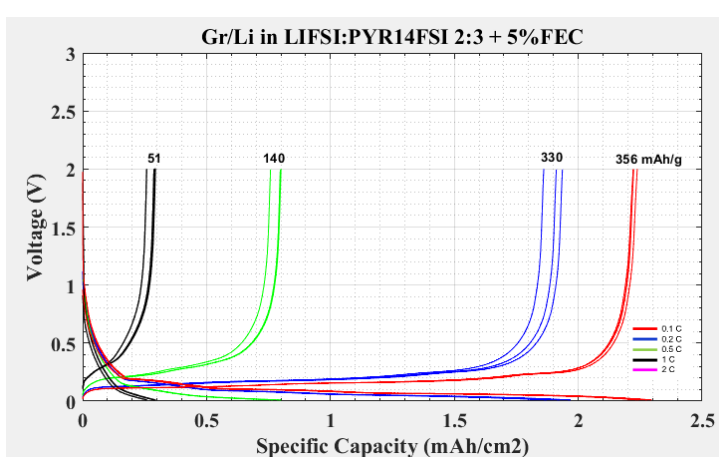
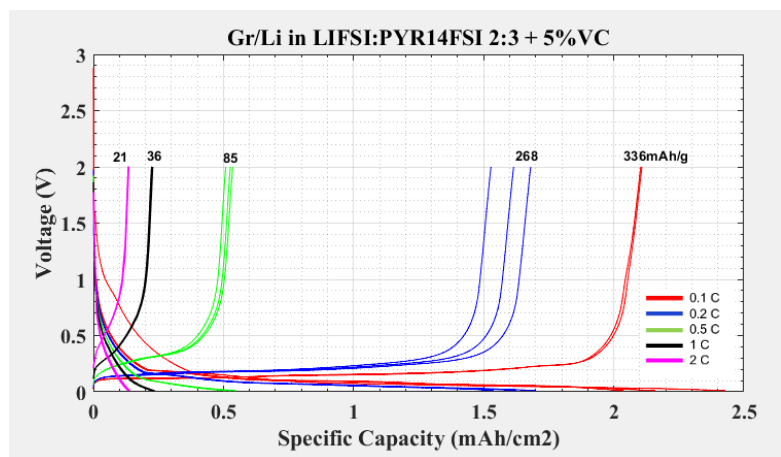


Figure 3-3: Charge/Discharge cycling at different C rate of anode half cells in $\text{LiFSI:PYR}_{14}\text{FSI } 2:3$ ionic liquid electrolyte with (a) VC additive (b) FEC additive

The charge-discharge curves presented in Figure 3-2 reveal that the organic electrolyte containing VC and FEC additives demonstrated first cycle coulombic efficiencies of 89.8%

and 91.36%, respectively. The cycling data at various C-rates indicates that cells containing the FEC additive exhibit a lower capacity drop at higher C-rates compared to those with the VC additive.

In the case of ionic liquid electrolytes (Figure 3-3), cells with VC and FEC additives showed first cycle coulombic efficiencies of 86.61% and 88.20%, respectively. Again, the electrolyte containing FEC exhibits better capacity retention at higher C-rates. These results suggest that FEC is more effective than VC in reducing irreversible capacity loss during the first cycle by forming a stable SEI layer on the electrode surface. This stabilization minimizes lithium loss, leading to improved first cycle efficiency and enhanced cycling performance compared to VC. The superior performance of FEC is consistent across both organic and ionic liquid electrolyte systems, particularly in terms of first cycle efficiency and capacity retention at higher C-rate.

The reduction potential of FEC (~ 1.6 V vs. Li/Li^+) is higher than that of VC (~ 1.3 V vs. Li/Li^+) [26]. This earlier SEI formation with FEC enables rapid passivation of the anode surface, minimizing parasitic reactions between the electrolyte and the electrode. VC's lower reduction potential delays SEI formation, allowing prolonged electrolyte decomposition at the anode interface during the initial lithiation phase. Consequently, while FEC consumes more lithium upfront, its faster passivation reduces cumulative lithium losses over the entire first cycle. Therefore, we add 5%FEC additive in all the electrolytes we use to carry out the electrochemical cycling study of the Li-ion full cells.

3.2 Initial Electrochemical study of LFP/Gr battlet full cell in Ionic Liquid Electrolyte

We use $\text{LiFSI: PYR}_{14}\text{FSI 2:3} + 5\%\text{FEC}$ electrolyte to conduct a preliminary electrochemical cycling study of the battery in the proposed non-flammable ionic liquid electrolyte. Average power consumption for medical monitoring use (cases with lower sampling rates 100

Hz patches) is likely in the range of 4-8 mW for 24-hour operation. An LFP/Gr cell operating at 3.7V would require a capacity of $\frac{4-8 \text{ mW} \cdot 24 \text{ hrs}}{3.7 \text{ V}} = 26 - 50 \text{ mAh}$. Our aim here is to try to achieve an areal capacity of $>1 \text{ mAh/cm}^2$. So that we can scale this battlet battery area and achieve these desired capacity requirements.

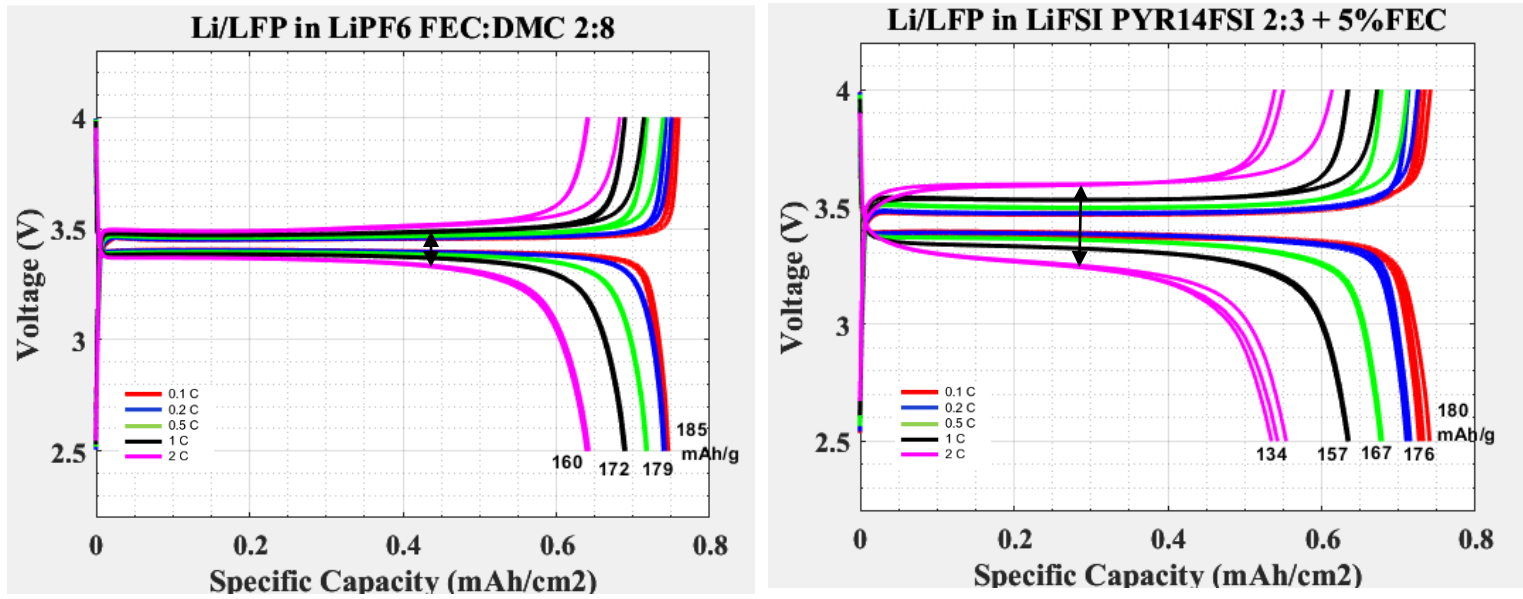


Figure 3-4: Charge/Discharge curves of cathode half-cell at different C rates in (a) organic liquid electrolyte and (b) ionic liquid electrolyte. Increase in polarization with increasing C-rate indicated by arrows.

To evaluate the electrochemical performance of individual battery materials like LFP and Graphite in the ionic liquid electrolyte, anode and cathode half-cells were assembled and tested under various charging and discharging rates ranging from 0.1C to 2C. The cathode, anode, and electrolyte in cathode half-cell were LFP (0.5 cm^2) / Li-metal (0.6 cm^2) / LiFSI:PYR₁₄FSI 2:3 (100 μL) + 5%FEC and in the case of anode half cell were Li-metal (0.6 cm^2) / Graphite (0.5 cm^2) / LiFSI:PYR₁₄FSI 2:3 (100 μL) + 5%FEC. LFP slurries were dispensed on Al foil to form 3x3 battlet electrodes with 4 mg/cm^2 of loading density, which provides an areal capacity of 0.7 mAh/cm^2 based on a theoretical capacity of 170 mAh/g for LFP. Therefore, the total theoretical capacity of the testing battery sample is 0.35 mAh . To

further compare the electrochemical performance of the ionic liquid with traditional organic electrolytes, coin cells in 1M LiPF₆ in FEC: DMC 2:8 electrolyte were also tested.

Figure 3-4 (a) and (b) show the charge and discharge curves at various C rates (C/10, C/5, C/2, 1C, and 2C) for the ionic liquid and organic electrolyte cathode half cells, respectively. Given a capacity of 0.7 mAh/cm², the corresponding currents densities at these three different C-rates are 0.07 mA/cm², 0.14 mA/cm², 0.35 mA/cm², 0.7 mA/cm², and 1.4 mA/cm², respectively. Each current rate is cycled 6 times. The results show that the ionic liquid battery provides 0.72 mAh/cm² at C/10, 0.7 mAh/cm² at C/5, 0.67 mAh/cm² at C/2, 0.62 mAh/cm² at 1C and 0.53 mAh/cm² at 2C rate. The reason for obtained specific capacity values to be more than theoretical capacity is because of the measured electrode weight negative deviation as addressed in Chapter 2. For the battery with 1M LiPF₆ FEC:DMC 2:8 electrolyte, capacities of 0.74 mAh/cm² at C/10 and C/5, 0.7 mAh/cm² at C/2, 0.68 mAh/cm² at 1C and 0.6 mAh/cm² at 2C were obtained. Greater polarization is observed in the ionic liquid electrolyte battery as indicated by the increased overpotential and sloping feature of the redox plateau at higher C rates as shown with the arrows in the Figure 3-4.

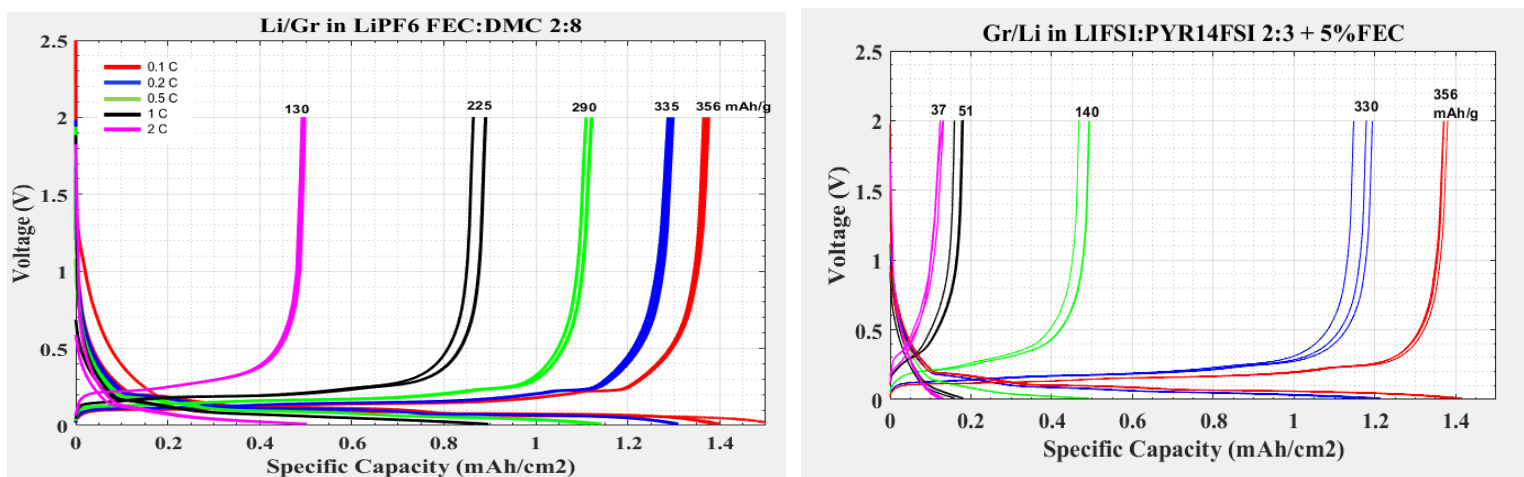


Figure 3-5: Charge/Discharge curves of anode half cells at different C rates in (a) Organic electrolyte (b) ionic liquid electrolyte

Figure 3-5(c) and (d) show the charge and discharge curves at various C rates (C/10, C/5, C/2, 1C, and 2C) for the ionic liquid and organic electrolyte anode half cells, respectively. The anode battlet electrodes were 3.7 mg/cm^2 of loading density, which is equivalent to 1.4 mAh/cm^2 of areal capacity (theoretical capacity of graphite 372 mAh/g). The first cycle coulombic efficiency in case the organic and ionic liquid electrolyte are 91.36% and 86.95% respectively. The capacity decay at higher C-rates in case of organic liquid electrolyte is also significantly smaller when compared to the ionic liquid electrolyte.

A similar performance difference is observed while cycling a LFP/Gr full cell. Figures 3-6 (a) and (b)-(c) show a full cell's charge discharge curve in organic electrolyte and ionic liquid electrolyte respectively at various C rates as discussed previously. The components of the full cell are LiFePO_4 (0.5 cm^2) cathode/ $\text{LiFSI}:\text{PYR}_{14}\text{FSI}$ 2:3 + 5%FEC ionic electrolyte or 1 M LiPF_6 EC:DMC 1:1 organic electrolyte (100uL)/ Graphite (0.5 cm^2) anode. As discussed in a full cell the capacity is decided by the loading density of the cathode. The full cell battlet cathode in organic electrolyte and ionic liquid electrolyte (Figure 3-6 (a) and (b)) have a loading density of 7.1 mg/cm^2 which is equivalent to 1.2 mAh/cm^2 of areal capacity. The N/P ratio is maintained as 1.2 in both the cells. Figure (c) shows the charge/discharge curve of battlet full cell in ionic liquid electrolyte of areal capacity 0.8 mAh/cm^2 . The thickness of the cathode in case of 1.2 mAh/cm^2 loading is $55\text{-}60 \mu\text{m}$ and the one with 0.8 mAh/cm^2 loading is $30 \mu\text{m}$.

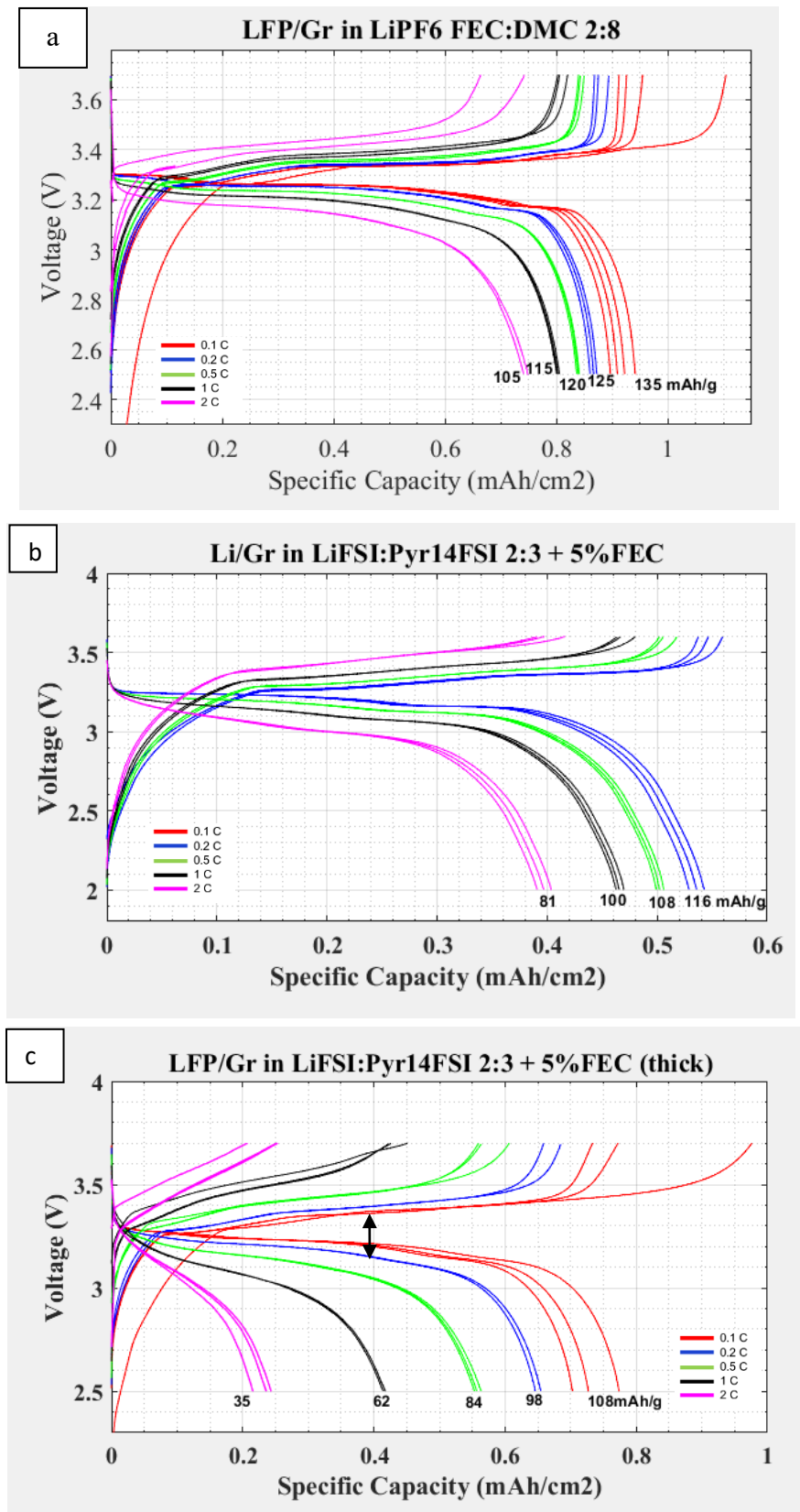


Figure3-6: Charge/Discharge curves of LFP/Gr full cells in (a) organic electrolyte (cell capacity 1.2 mAh/cm²) (b) ionic liquid electrolyte (cell capacity 1.2 mAh/cm²) (c) ionic liquid electrolyte (lower cell capacity 0.8 mAh/cm²)

The difference between cells (b) and (c) lies in the thickness of the electrode, with both having a constant area of 0.5 cm². This results in different areal capacities: 1 mAh/cm² for the thicker electrode in cell (b) and 0.8 mAh/cm² for the thinner electrode in cell (c). The charge/discharge curve for the thinner electrode (c) shows a higher specific capacity of 116 mAh/g at 0.2C compared to 98 mAh/g for the thicker electrode at the same rate. This demonstrates the impact of electrode thickness on lithium-ion diffusion and, consequently, on the cycling performance of the cell when using an ionic liquid electrolyte (Figure 3-7). The first cycle coulombic efficiency (FCE) of cell with organic electrolyte and ionic electrolyte are 85.16% and 81.14% respectively. A higher FCE means a greater proportion of the charge stored during the first cycle is recoverable during subsequent charge-discharge cycles. A lower FCE often points to significant electrolyte decomposition during the first cycle to form a SEI which affects the stability and the quality of the SEI formed and this will in turn affect the cycling performance in the further cycles at higher C-rates. The difference in the % capacity retention at various C-rates is more pronounced in ionic liquid electrolyte when compared to organic electrolyte as seen in Figure 3-7.

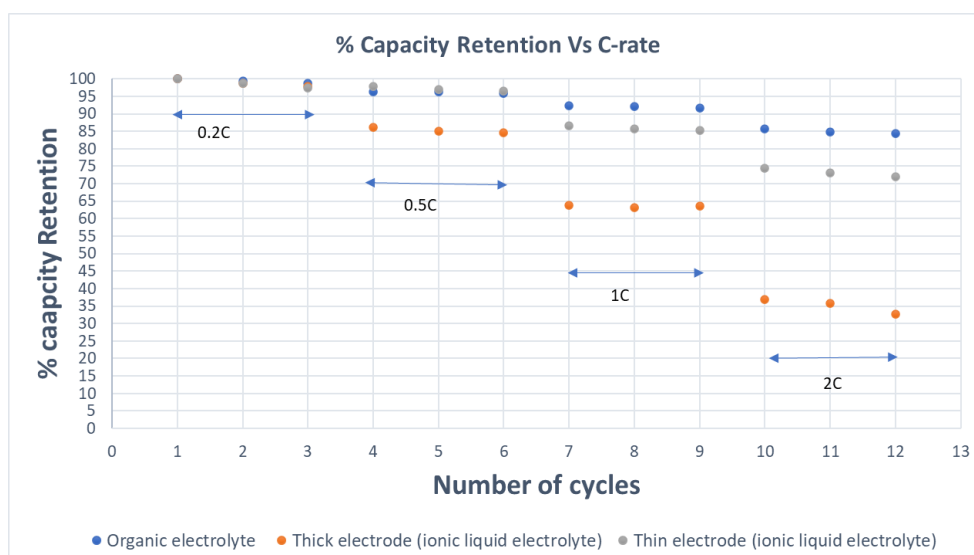


Figure 3-7: %Capacity retention comparison at various C-rates for ionic liquid electrolyte and ionic liquid electrolyte.

Considering the above testing results, including capacity, capacity decay rate, and columbic efficiency on both ionic liquid electrolyte and organic electrolyte, we find that the electrochemical performance is lower than the organic electrolyte. The main reason for this is due to ionic liquid electrolyte having lower ionic mobility (ionic conductivity) than conventional organic electrolyte due to higher viscosity of the solvent at room temperature. Low ionic conductivity leads to higher interface resistance causing high impedance and polarization in the cell and in turn leading to poor cycling performance. Hence a full cell designed for 1.2mAh/cm^2 of areal capacity delivers a maximum of 0.75mAh/cm^2 (62% of theoretical capacity) and 0.95mAh/cm^2 (80% of theoretical capacity) capacity in case of ionic liquid electrolyte and organic electrolyte respectively. And a full cell designed for 0.8mAh/cm^2 (electrode thickness of $30\text{ }\mu\text{m}$) delivers a maximum of 80% of theoretical capacity in ionic liquid electrolyte because the Li^+ diffusion in thinner electrode is less sluggish than thick electrode. But in this cofacial cell design only way to increase the areal capacity is by increasing the electrode thickness. Hence, in the next part we try to change the physico-chemical properties of the ionic liquid electrolyte to improve the areal capacity and cycling performance of the flexible battlet full cell.

3.3 Effect of salt concentration (LiFSI) in ionic liquid electrolyte on the cycling performance of Li-ion battery

Among all factors that affect the charging of a battery, electrolyte dominates the operating voltage, rate and cycle performance, temperature range as well as safety. In the next part of the study, we investigate the effect of LiFSI concentration in IL electrolyte on the performance of the battery. In addition, we also we evaluate the effect of cation type in the ionic liquid on the electrochemical cycling performance of the Li-ion battery. For this study we test the electrochemical performance of the IL electrolytes listed in Table 3-1. We do not

change the salt (LiFSI) and use FSI anion based ionic liquid as the FSI based system exhibits superior properties in terms of viscosity, ionic conductivity and wide electrochemical window when compared to other anion-based systems as discussed in Chapter 1 (Table 1-5).

Electrolyte	Ionic Conductivity mS/cm @ 25°C	Viscosity mPa s @ 25°C	Li/LiFSI molarity
Organic LiPF ₆ in EC/DMC	10.9	Low	1 M
LiFSI : PYR ₁₄ FSI (2:3 mole ratio)	1.6	170.8	2.14 M
LiFSI : PYR ₁₄ FSI (1:9 mole ratio)	4.5	67	0.43 M
LiFSI : EMIMFSI (1:9 mole ratio)	13.2	25.14	0.5 M
LIFSI:EMIMFSI (2:3 mole ratio)	4.7	90	2.3 M

Table 3-1: Physico-Chemical properties IL electrolytes with varying molar concentrations [27][28]

The concentration of the salt and ionic solvent in the ionic electrolyte as well as the type of ions in the ionic liquid can affect the physico-chemical properties of the ionic liquid electrolyte. Larger cation size of Pyr₁₄⁺ when compared to Emim⁺ hinders the quick ionic diffusion of Li⁺ and hence affects the ionic conductivity of the electrolyte [29]. Lower the concentration of the salt compared to the ionic liquid lower the viscosity of the electrolyte, which also improves the ionic conductivity of Li⁺. But lower the salt concentration will decrease the overall concentration of the Li⁺ (lower Li⁺ transference number) in the electrolyte which will affect the ionic conductivity of the ionic liquid electrolyte as shown in Table 3-1. Hence a good balance between the molar concentration and type of the cation used is to be determined for better cycling performance.

We will first discuss about the effect of salt concentration in ionic liquid electrolyte on the electrochemical performance of the Li-ion battery. We focus on its effect on the anode in particular as it can greatly affect the anode capacity and SEI formation compared to cathode cycling performance.

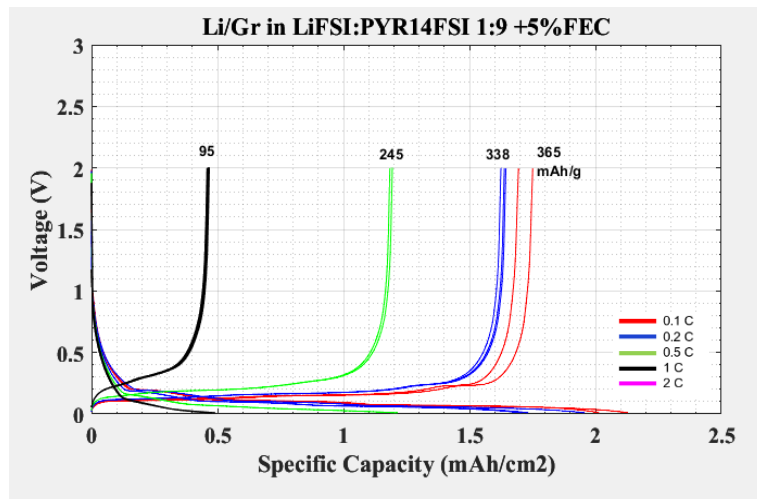
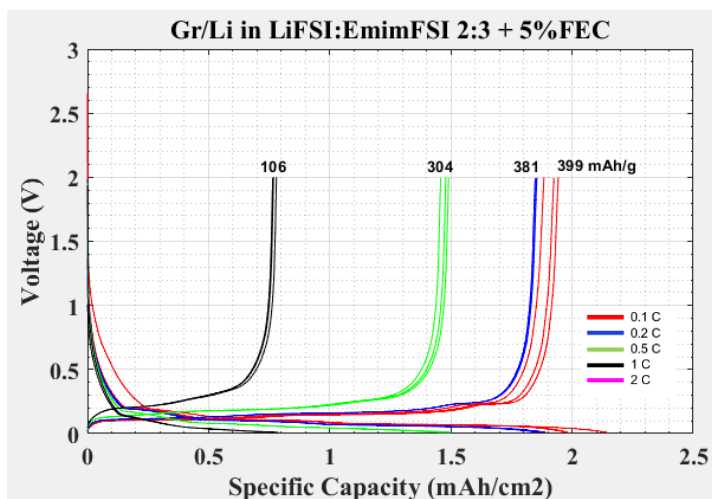


Figure 3-8: Charge/discharge of anode half-cell in IL electrolyte (a) LiFSI: EmimFSI 2:3 + 5%FEC (b) LiFSI: EmimFSI 1:9 + 5%FEC

Figure 3-8 (a) and (b) shows the charge discharge curves of anode half-cell in LiFSI: EmimFSI 1:9 (Low concentration electrolyte LCE) and LiFSI: EmimFSI 2:3 (High concentration electrolyte HCE) ionic liquid electrolyte. 5% FEC additive was used in both the electrolytes. The anode battlet electrodes were 4.8 mg/cm^2 of loading density, which is equivalent to 1.7 mAh/cm^2 of areal capacity (theoretical capacity of graphite 372 mAh/g). As discussed in chapter 1, due to error while measuring the weight of the battlet the specific capacity value exceeds 372 mAh/g but their comparison is still accurate as the electrodes are made from the same print batch with the same blank weight. The LCE and HCE system shows a first cycle efficiency of 79.61% and 87.83% respectively.

Figure 3-8 (a) and (b) shows that the difference in capacity and capacity decay with the increasing C rate is drastic in the case of lower molar ratio LiFSI: EmimFSI 1:9 electrolyte when compared to 2:3 molar ratio. A similar trend is observed in the case of LiFSI: PYR₁₄FSI ionic liquid electrolyte system too as shown in the % coulombic efficiency curves of their anode half cells in Figure 3-9.

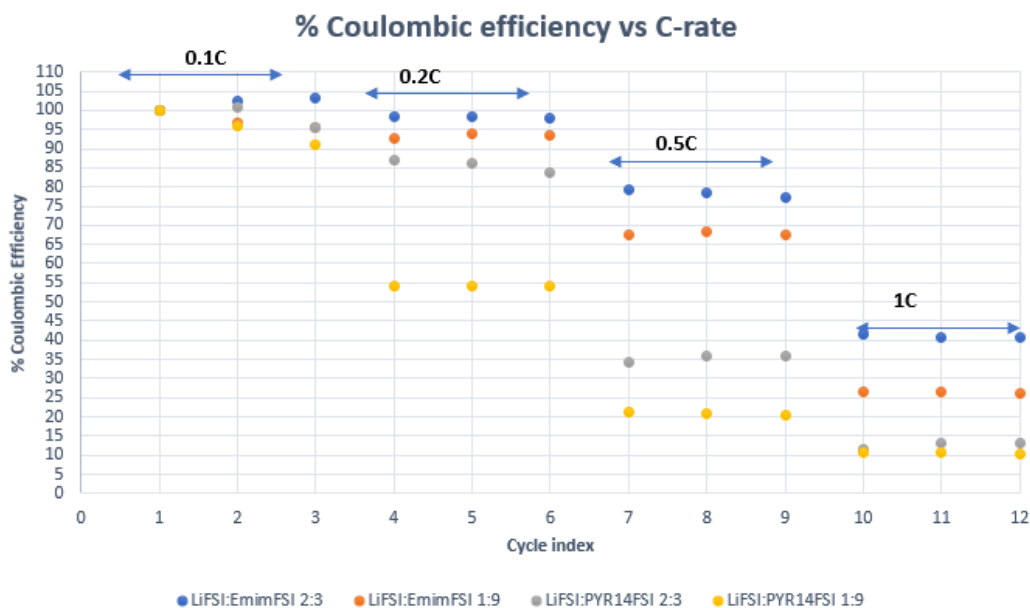


Figure 3-9: %Capacity retention comparison at various C-rates for HCE and LCE ionic liquid electrolyte with Pyr14⁺ and Emim⁺ cation containing ionic liquid.

Despite the lower ionic conductivity and higher viscosity of HCE compared to LCE, the Li⁺ ions in HCE form monodentate coordination with the ionic liquid anions as shown in figure 3-10. This weaker solvation of lithium ions with the solvent ions minimizes the solvent co-intercalation into the electrode material [30][31]. In contrast, the Li⁺ ions in LCE form bidentate coordination with the anions, resulting in stronger solvation structure leading higher availability of free solvent molecules (cation) that can intercalate along with the Li⁺ into the graphite layers, increasing the likelihood of co-intercalation as shown in Figure 3-10.

Monodentate coordination structures around lithium ions are more compact, reducing the likelihood of co-intercalation due to size constraints. Higher concentrations of Li salt in HCE lead to larger lithium-ion transfer numbers. In HCE, anions are more likely to be incorporated into the primary solvation shell of lithium ions, facilitating the formation of an anion-derived solid electrolyte interphase (SEI) upon reaching the anode surface as shown in Figure 3-10. This SEI is stable, exhibits lower charge transfer resistance, and offers higher conductivity compared to the SEI formed primarily by solvent molecules in LCE [32] [33].

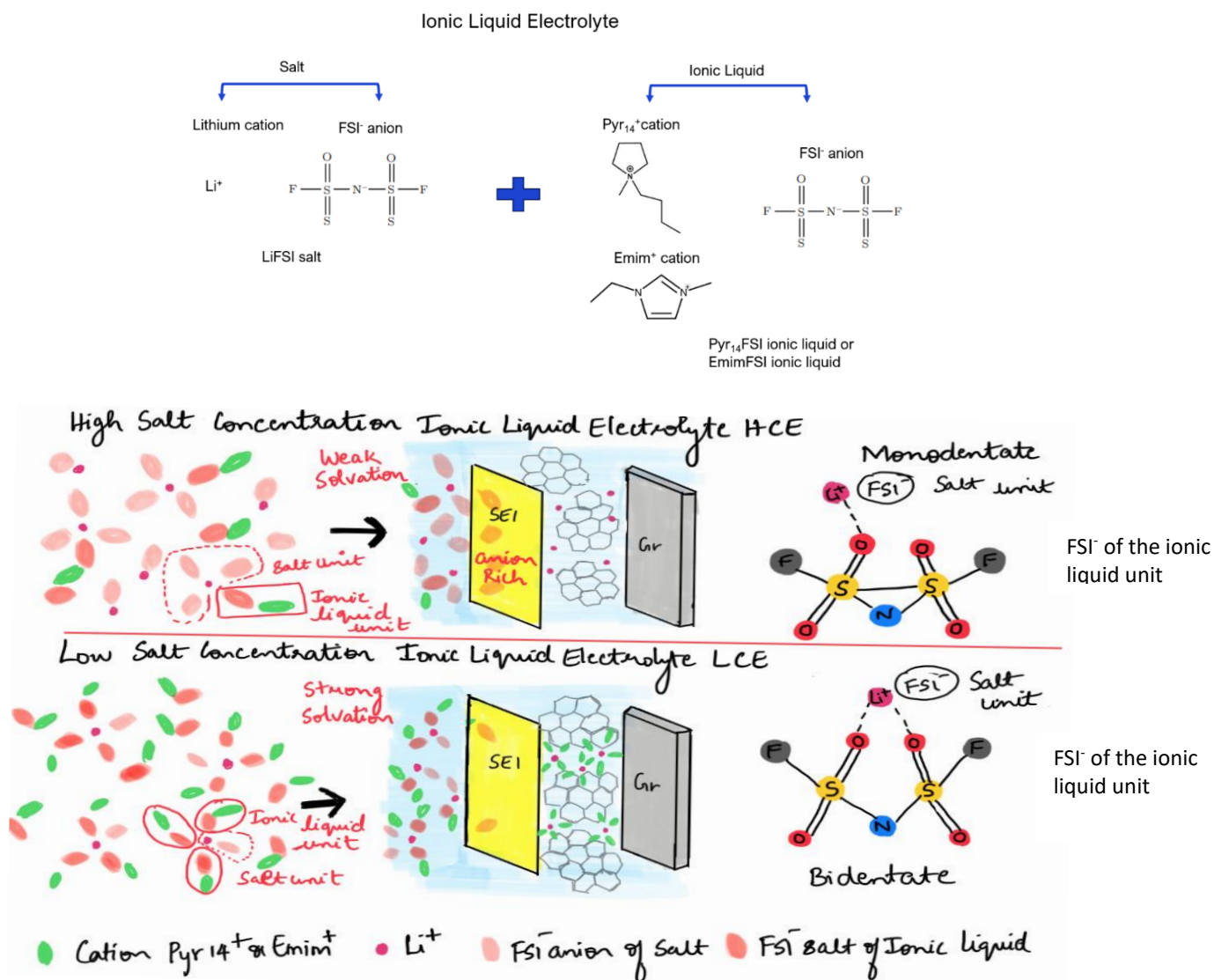


Figure 3-10: Solvation structure of Li⁺ in case of HCE and LCE. Demonstration of solvent co-intercalation into graphite in case of low concentration electrolyte (LCE).

The formation of SEI depends heavily on the reductive reactions of the electrolyte at the electrode surface. Poor SEI quality results in continuous electrolyte decomposition, leading to low coulombic efficiency, solvent intercalation into the graphite interlayers, capacity degradation, and cycling instability. The ability of Li⁺ ions to desolvate upon reaching the electrode depends on their coordination structure (Li⁺ solvation structure). When desolvation is inefficient, lithium ions enter the graphite layers along with solvent molecules, causing graphite exfoliation. This happens in the case of LCE electrolyte as shown in Figure 3-10.



Left → 2:3 molar ratio of ionic liquid
Right → 1:9 molar ratio Ionic Liquid

Figure 3-11: Opened anode half cells cycled in low salt concentration IL electrolyte (right) and high salt concentration IL electrolyte (left)

According to the literature, Li plating is observed on the graphite surface in cells with LCE after cycling, contributing to high-capacity decay [34]. In contrast, the anion-derived SEI formed in HCE effectively inhibits Li plating and enhances cycling stability. Figure 3-11 shows the image of opened graphite half cells after being cycled in LiFSI:EmimFSI 1:9 and LiFSI:EmimFSI 2:3 ionic liquid electrolyte. A brown residue is observed in cell cycled in LCE which is due to the exfoliation of graphite caused by the co-intercalation of solvent into the graphite [34]. Hence using a 2:3 molar ratio ionic liquid electrolyte is preferable to achieve good coulombic efficiency and capacity retention at various C rates.

3.4 Effect of cation type in the solvent of the ionic liquid electrolyte on the cycling performance of the Li-ion battery

Next, we investigate the effect of the cation type in ionic liquid on the performance of the full cell in ionic liquid electrolyte. For this study we use higher salt concentration electrolyte; LiFSI:EmimFSI 2:3 and LiFSI:Pyr₁₄FSI 2:3 as HCE exhibits better cycling performance compared to LCE as discussed in the previous section. The Emim⁺ cation has a planar imidazolium ring structure with shorter ethyl side chain, while the Pyr₁₄⁺ cation has a non-planar pyrrolidinium ring with longer butyl side chain. Hence Emim⁺ is smaller in size

compared to Pyr_{14}^+ , this size disparity results in Emim^+ containing electrolyte having higher conductivity and lower viscosity which leads to higher diffusion coefficient benefiting the battery's rate capability.

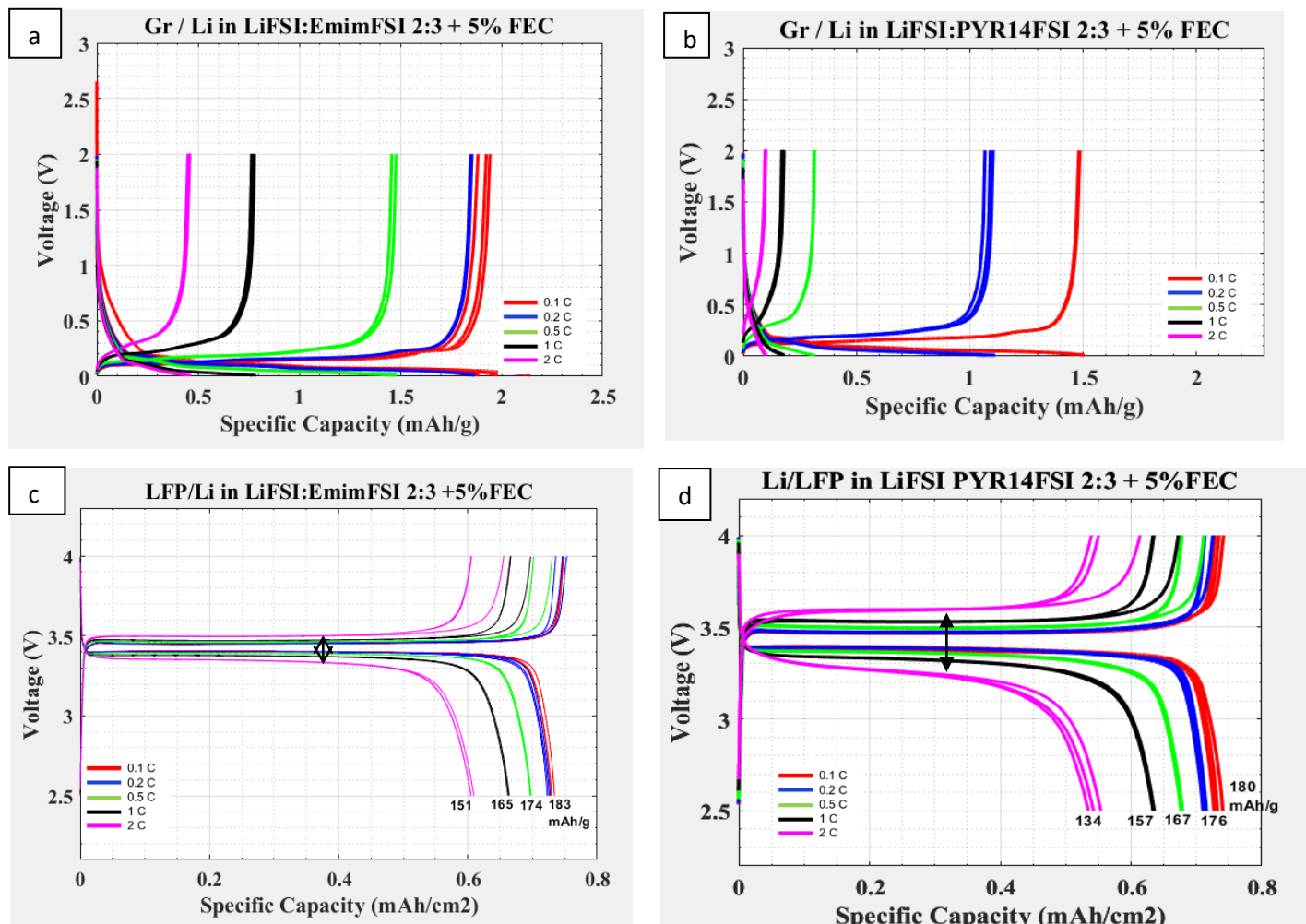


Figure 3-12: Charge/discharge curve of anode half-cell in (a) LiFSI: EmimFSI 2:3 IL electrolyte (b) LiFSI:Py₁₄FSI 2:3 IL electrolyte. Charge/discharge curve of cathode half-cell in (c) LiFSI:EmimFSI 2:3 IL electrolyte (d) LiFSI:Py₁₄FSI 2:3 IL electrolyte.

The Emim^+ exhibits less coordination with the FSI^- anion (3.6 coordination number) compared to Pyr_{14}^+ with FSI^- (4.4 coordination number) [35]. This reduced coordination allows for better availability of anions to participate in SEI formation resulting a more stable SEI at the anode electrode surface. This can be seen in the % coulombic efficiency curve in

Figure 3-9 and in the anode half-cell charge/discharge curves in Figure 3-12, which are designed for 1.7mAh/cm² areal capacity. Figure 3-12 shows that the Emim based electrolyte shows higher capacity retention, lower polarization and cycling stability over various C-rates when compared to the Pyr14 based ionic electrolyte.

A similar performance difference in the LFP/Gr full cell containing Emim⁺ and Pyr14⁺ ionic liquid electrolytes was observed, mirroring the results from the anode and cathode half-cells. Figure 3-13 compares the charge-discharge curves of full cells with a 9.4 mg/cm² cathode loading density, equivalent to 1.6 mAh/cm² of areal capacity, using LiFSI:EmimFSI 2:3 and LiFSI:Pyr₁₄FSI 2:3 ionic liquid electrolytes. Both electrolytes contained 5% FEC additive, and an N/P ratio of 1.2-1.3 was maintained.

The imidazolium (Emim) based cell achieved 76% of theoretical capacity, outperforming the pyrrolidinium (Pyr14) based cell, which reached 68% of theoretical capacity. The first cycle efficiency (FCE) for LiFSI:EmimFSI 2:3 and LiFSI:Pyr₁₄FSI 2:3 ionic liquid electrolyte cells was 81.56% and 79.2%, respectively. This indicates that less lithium (capacity) is lost during SEI formation in the Emim ionic liquid electrolyte-based cell, resulting in more capacity available for subsequent cycles. The Emim-based system also demonstrated lower capacity drop and lower polarization at higher C-rates, as shown in Figure 3-13 (b).

Although the capacity of the Emim-based cell at 0.1C is close to that of the organic system, its capacity at higher C-rates is lower compared to organic electrolytes, as seen in Figures 3-6 and 3-13(b). This difference is attributed to the typical characteristics of ionic liquids, including lower Li⁺ conductivity, higher viscosity, higher interfacial resistance, and solvation effects.

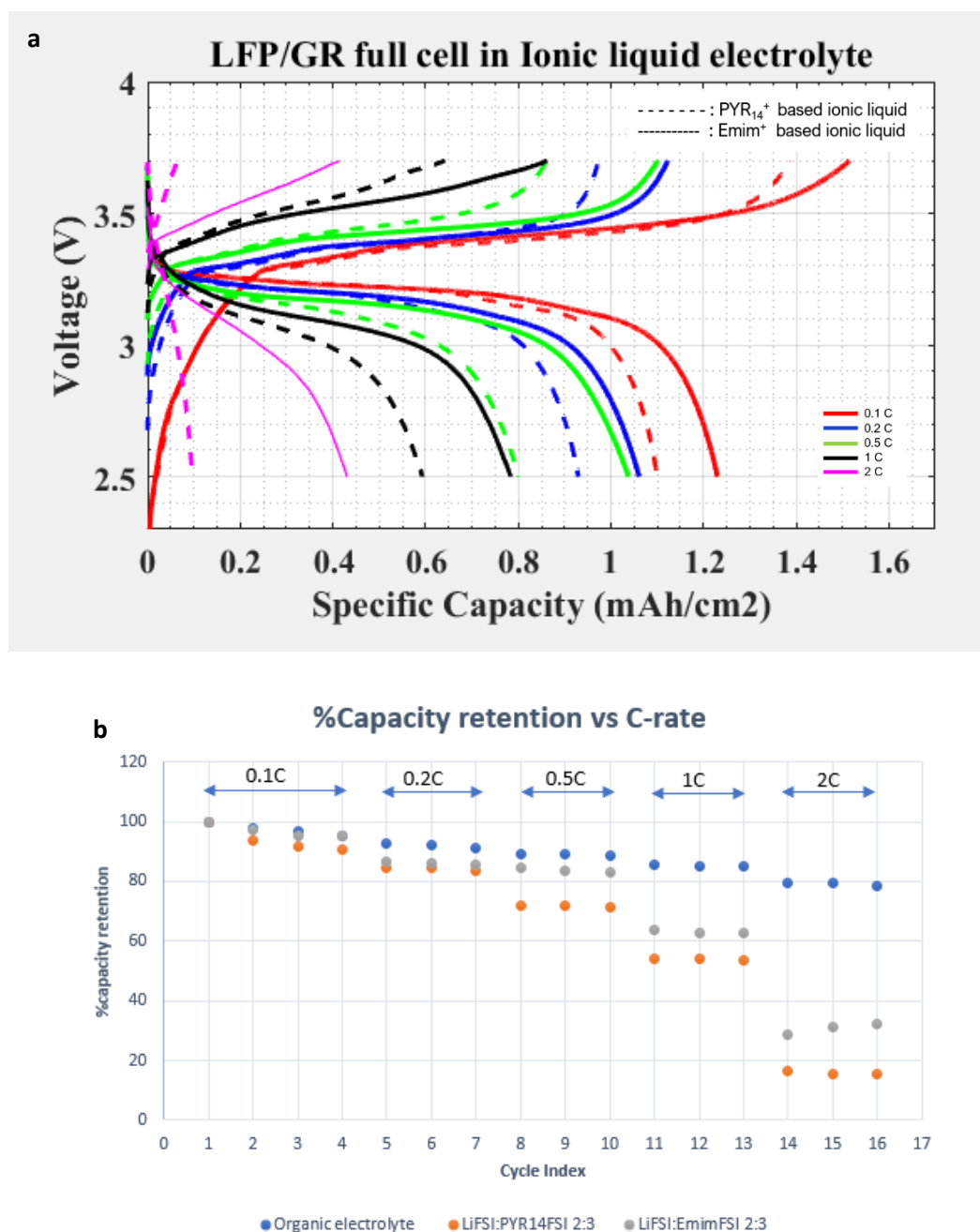


Figure 3-13: Comparison of (a) areal capacity (b)cycling performance of LFP/Gr full cell in Emim and Pyr₁₄ based ionic liquid electrolyte.

In conclusion, the imidazolium-based ionic liquid electrolyte proves to be a better alternative than the previously used pyrrolidinium-based ionic liquid electrolyte for achieving good capacity retention and cycling stability in LFP/Gr cells. While not matching the performance of organic electrolytes at higher C-rates, it offers the advantages of non-flammability and enhanced safety. In the cofacial battery design, optimizing the properties of ionic liquid

electrolytes can enhance cycling performance—but primarily in cells with thinner electrodes. For high areal capacity cells with thicker electrodes, improving cycling performance may be better achieved by exploring alternative non-flammable electrolytes or adopting different cell geometries.

CHAPTER 4: INTERDIGITATED CO-PLANAR LI-ION BATTERY

4.1 Motivation and Development of Coplanar Interdigitated Li-ion Battery

Flexible lithium-ion batteries (LIBs) have emerged as a crucial component in the development of flexible hybrid electronics (FHE) applications. Our previous research demonstrated a battlet design of cofacial flexible LIBs with a total thickness under 300 μm and electrode thickness of 50-60 μm , capable of delivering a peak capacity of 0.75 mAh/cm² (theoretical capacity of 1.2mAh/cm²) of in an ionic electrolyte while withstanding 1000 bending cycles at a 5 mm bending radius [36]. And this was improved to 76% theoretical capacity by changing the ionic liquid chemistry. However, increasing the thickness to achieve higher loading density and areal capacity leads to lower peak capacity and poor cycling performance at higher C rates as seen in the previous chapter.

The cofacial battlet design presents challenges such as potential misalignment of the anode and cathode during packaging, which can lead to lithium plating. This lithium plating can subsequently result in capacity loss and battery failure over time or shorting of the battery as the Li dendrites pierce through the separator as shown in Figure 4-1. Additionally, thicker electrodes in this configuration can impede ionic transport and compromise flexibility, restricting the achievable loading density. These limitations have prompted exploration of alternative cell configurations where the Li⁺ diffusion path differs from that in the traditional cofacial design.

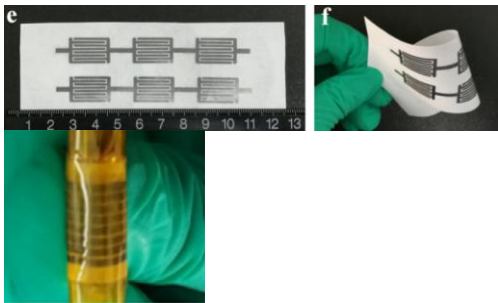
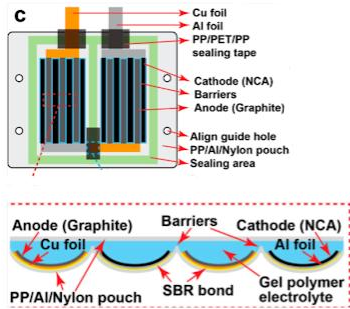
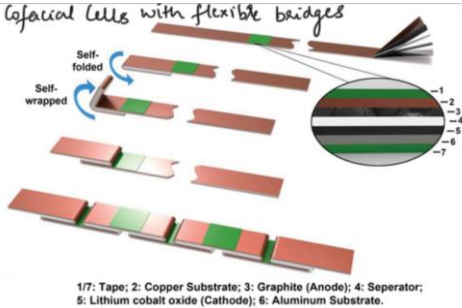
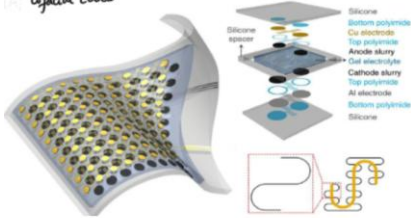
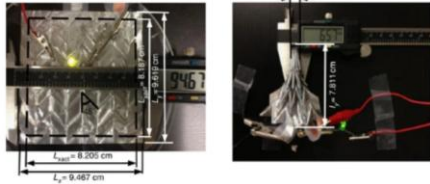


Figure 4-1: (a) Misalignment of the co-facial electrodes causing formation and growth of Li dendrites over time; (b) shorting of battery due to puncture of separator by the Li dendrites [37]

The performance of lithium-ion batteries is fundamentally governed by the interplay between electrode architecture and ionic transport kinetics. In cofacial LIBs, where electrodes are stacked in a layer-by-layer configuration, the Li^+ diffusion path length scales with electrode thickness. As electrodes thicken, the ionic resistance increases quadratically due to elongated solid-state diffusion pathways within the active material matrix [38]. The active surface for ionic diffusion does not scale with the increase in thickness as well. Electrolyte infiltration becomes challenging for thick electrodes in cofacial designs, creating regions of low ionic conductivity. This issue is exacerbated in the case of ionic liquid electrolytes, which inherently have lower ionic conductivity and high viscosity.

In contrast, the interdigitated coplanar layout generates uniform electric field distributions across electrode widths, unlike cofacial configurations where field strength decays exponentially with depth from the separator. Finite-element simulations reveal that coplanar cells maintain field homogeneity across electrode fingers of a given width, compared to thick cofacial electrodes with a similar thickness as the width of the interdigitated electrode. This homogeneity promotes synchronous Li^+ intercalation along the entire electrode perimeter, reducing localized overpotentials [39]. Also, the Li^+ diffusion path length is fixed as the electrode thickness scales.

Various designs have been explored to fabricate flexible Li-ion batteries as listed in Table 4-1. Most of these designs except the interdigitated designs exhibit good flexibility but are complex to manufacture and since they have cofacial electrodes their cell capacity is also limited by the thickness of the electrodes. Research on coplanar interdigitated battery designs has shown promise in terms ease of fabrication and cycling performance, but these are limited by areal capacity due to electrode thickness constraints of less than $7\text{ }\mu\text{m}$ [42] and if the electrodes are thicker, they offer flexibility in only one bending direction [43] as shown in Tabel 4-1.

Electrode Design	Comments	Designs
Coplanar Interdigitated [42]	Excellent flexibility due to very low electrode thickness Low cell capacity <0.1 mAh/cm ²	
Coplanar Interdigitated [43]	Improved cell capacity 0.5 mAh/cm ² Flexibility in only in one bending direction	<p>Coplanar cells</p> 
Island bridge Zig-zag pattern [44]	Complex fabrication Bending based on the fold design. Bending only in one direction. Limited durability	<p>Coplanar cells with flexible bridges</p> 
Island bridge Serpentine pattern [49]	Good flexibility and cell capacity Difficult to fabricate stretchable batteries Incompatible with liquid electrolyte	<p>Coplanar cells</p> 
Miura fold (Origami Kirigami design) [45] [46]	Excellent flexibility Complex fabrication and limited durability.	<p>Coplanar cells with flexible Pattern</p> 

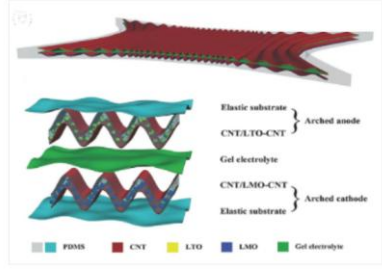
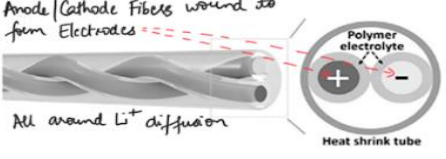
Wavy electrode [47]	Excellent stretchability Complex fabrication Lower cell capacity	Cofacial pre-strained electrodes 
1D and textile [48]	Excellent flexibility Low cell capacity and complex fabrication	Anode/Cathode Fibers wound to form Electrodes All around Li^+ diffusion 

Table 4-1: Electrode designs in flexible lithium-ion batteries [40][41]

To overcome these limitations, we propose adopting the battlet approach in a coplanar interdigitated structure, where the anode and cathode battlets are interdigitated and positioned on the same plane with a certain pitch as shown in Figure 4-2(b). This innovative design not only reduces stress concentration during bending but also offers several advantages over existing configurations. These include enhanced flexibility in all directions, increased mass loading without cracking during bending, elimination of the separator, scalability of electrode dimensions leading to a reduced form factor, and improved safety through the use of ionic electrolytes.

In this structure, the width of each electrode is shared by two adjacent electrodes, thus reducing the Li^+ diffusion distance. As the diffusion path of Li^+ in the interdigitated design is now lateral, thicker electrodes can be designed to achieve higher loading and areal capacity without increasing the Li^+ diffusion distance. By addressing the shortcomings of previous designs, our proposed coplanar interdigitated battlet structure aims to advance the development of flexible LIBs for next-generation FHE applications.

We fabricate this structure on a flexible substrate using the FlexTrate™ platform [50], which will enable a readily integrable flexible Li-ion battery with novel packaging into the flexible

circuit like any other electronic Integrated Circuit (IC) element to form a functional wearable device as shown in Figure 4-2. This approach promises to overcome the limitations of traditional cofacial designs while offering improved performance and manufacturability for flexible lithium-ion batteries. This will enable development of an integrable energy platform that utilizes the otherwise unused or ‘blank’ spaces within the device packaging. Imagine a battery that flows around the edges of the smartwatch or one that conforms to the folds of a patch on your skin.

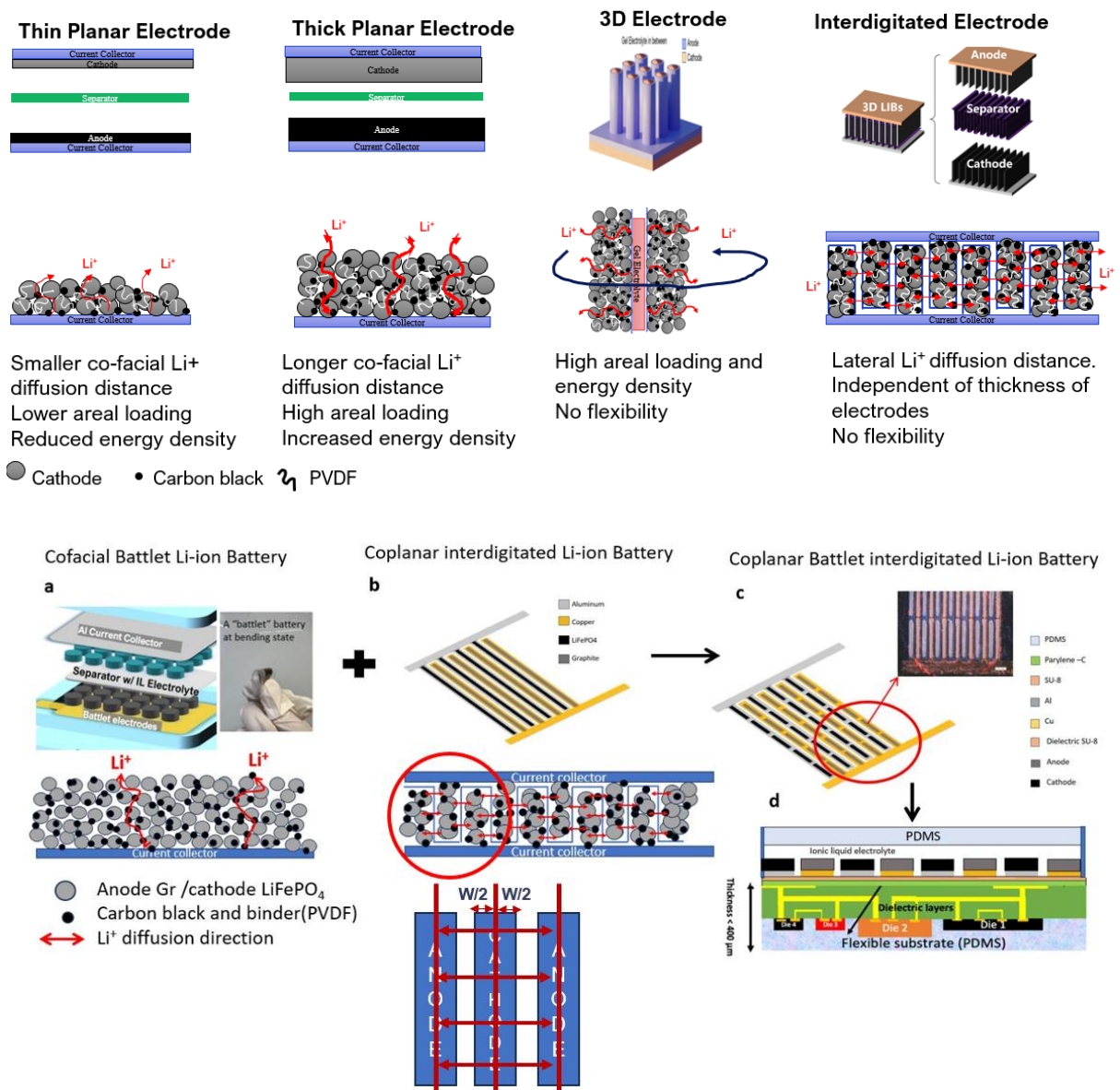
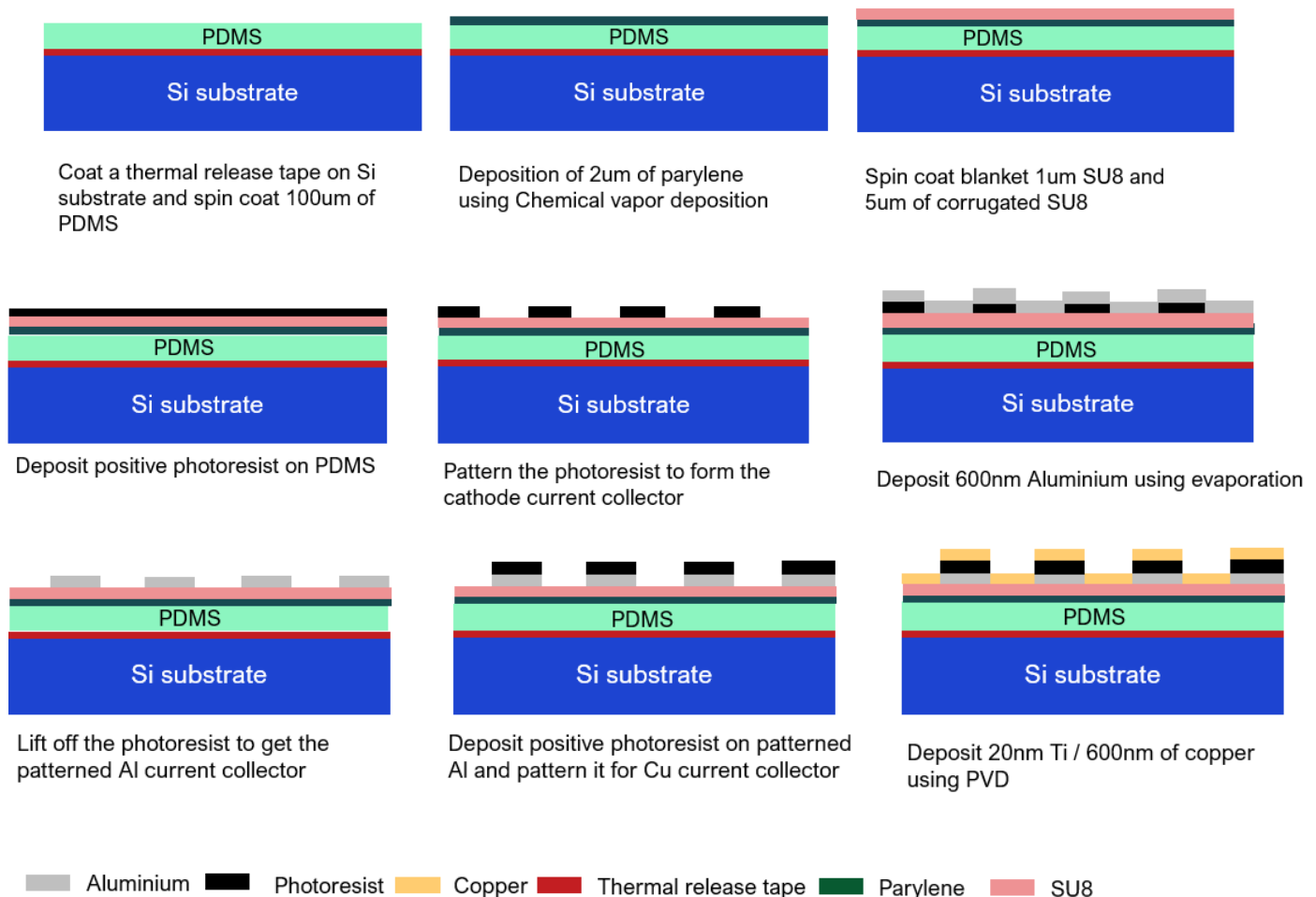


Figure 4-2: Li^+ ion diffusion path in cofacial and coplanar electrode design (Top) [39]; structure of proposed battlet interdigitated electrode (bottom)

4.2 Fabrication of Interdigitated Battlet Co-planar Battery on Flexible Substrate

Figure 4-3 shows the fabrication process of the interdigitated current collectors on Polydimethylsiloxane (PDMS) using FlexTrate™ process. Initially, a double-sided thermal release tape is laminated onto a 4-inch glass wafer. Then, uncured PDMS is spin-coated at 2000 rpm on the substrate and cured at room temperature. The PDMS coating is typically less than 150 μm thick. A 2 μm Parylene C layer is deposited on the PDMS via chemical vapor deposition as a buffer layer to mitigate the CTE mismatch of PDMS and current collectors. Next a 1 μm blanket SU8 photoresist is spin-coated followed by another 5 μm SU8 spin coating, which is corrugated. Subsequently, 20nm/600 nm of Ti/Al is evaporated on the SU8 as the cathode current collector. The sheet resistivity is 4 $\mu\Omega\cdot\text{cm}$ in evaporation of Al film. Simultaneously, a 20/600 nm Ti/Cu film is sputtered on another substrate as the anode current collector.



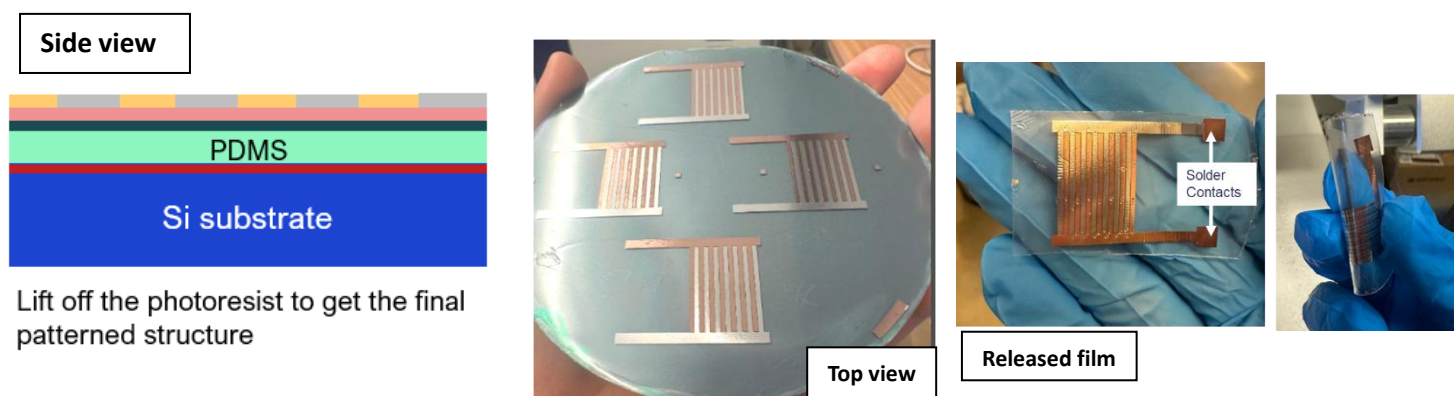


Figure 4-3: Fabrication process flow for interdigitated current collectors

Next the battery materials are deposited onto the flexible current collectors using the ink-jet printer. Figure 4-4 shows the complete cell configuration before sealing. In the interdigitated coplanar battlet configuration, the length and width of the current collectors (aluminum and copper) is $18,000\ \mu\text{m} \times 700\ \mu\text{m}$, with a $100\ \mu\text{m}$ spacing between them. The battlet design's cathode (LiFePO_4) and anode ($\text{Li}_4\text{Ti}_5\text{O}_{12}$), with a length of $6000\ \mu\text{m}$, width of $350\ \mu\text{m}$, pitch of $450\ \mu\text{m}$, and a thickness of up to $20\text{--}30\ \mu\text{m}$, are deposited as shown in Figure 4-4(c). The final design has 3X7 cathode and anode electrodes each. The height of the electrode in the case of LFP/LTO chemistry, where the theoretical capacity difference is not a lot (LFP -170 mAh/g and LTO- 160 mAh/g) slightly thicker LTO is deposited compared to LFP to maintain the N/P ratio between 1.2 – 1.4. The electrode width can vary based on the viscosity of the slurry which affects its spread on the current collector during printing process. Based on the particle size, nozzle diameter and minimum viscosity needed to print the slurry at present we print $350\text{--}400\ \mu\text{m}$ wide electrodes, which results in $150\text{--}200\ \mu\text{m}$ Li^+ diffusion distance during cycling. After that, the electrode slurry is vacuum dried at $100\ ^\circ\text{C}$ and later a PDMS well is created to dispense and hold the ionic liquid electrolyte in the electrode area, and the whole battery is hermetically sealed with PDMS sheet as shown in Figure 4-5. No separator is used in this battery design assembly. This battery design provides a combination of low thickness($<500\ \mu\text{m}$), high energy density, low form factor, and high flexibility.

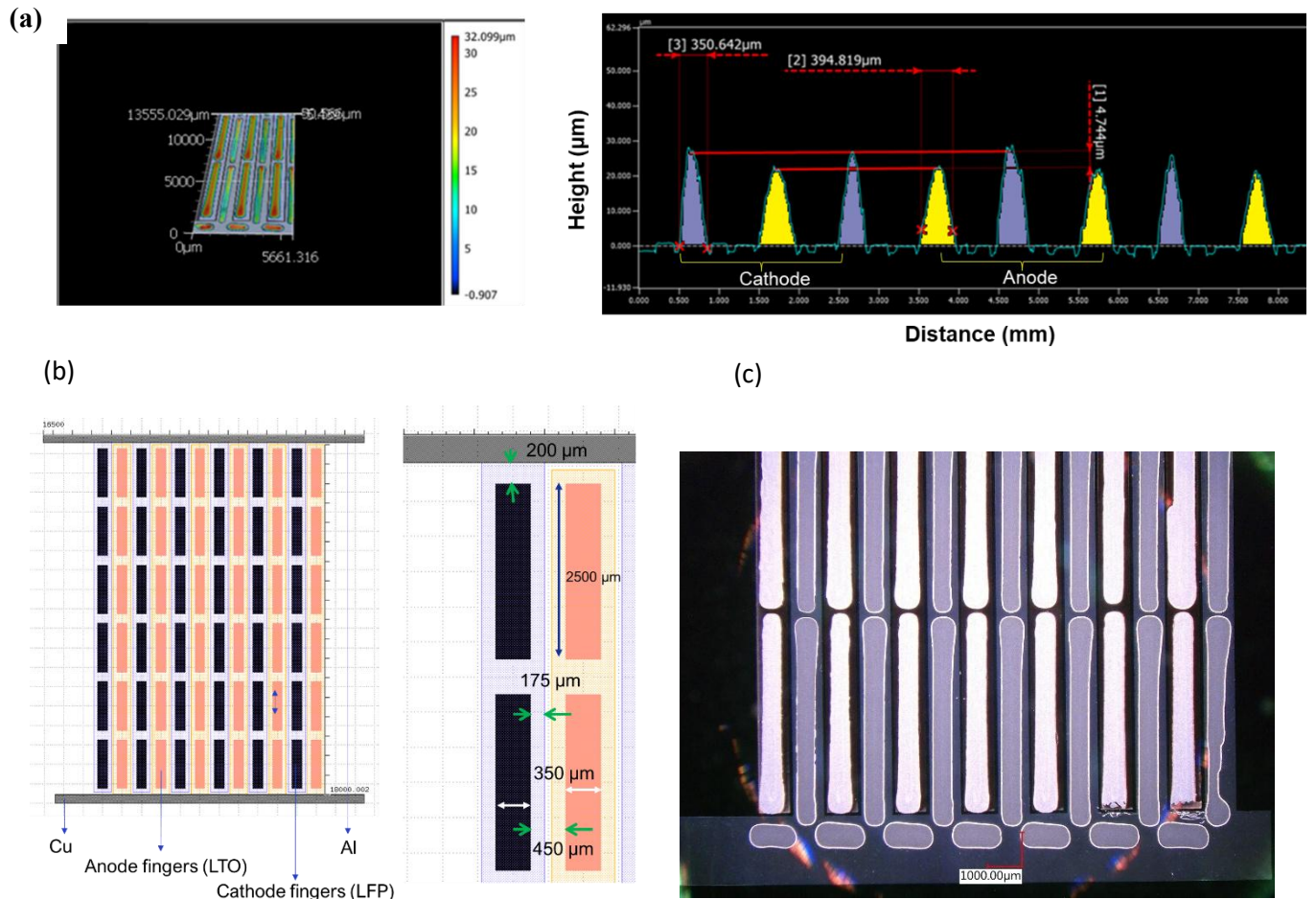


Figure 4-4: (a) Confocal microscope images of the surface profile of interdigitated battlet electrode.(b) Configuration of interdigitated current collectors and battlet electrodes. No of battlets not to scale (c) optical image of battlet electrodes.

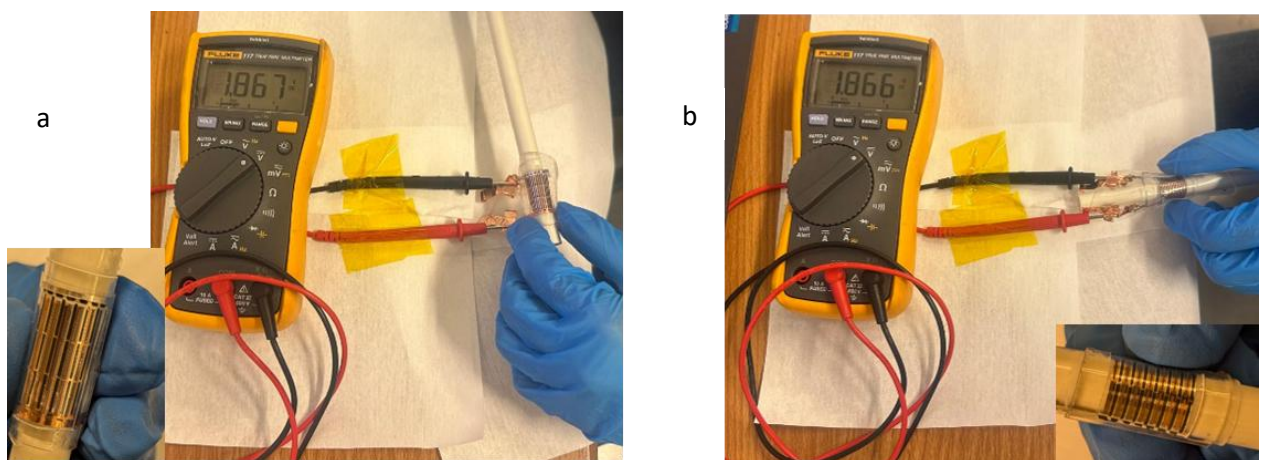


Figure 4-5: Packaged battlet interdigitated LFP/LTO battery in bent state after full charge at 0.1C (a) longitudinal bending (10mm bending radius) (b) lateral bending (10mm bending radius)

4.3 Electrochemical Cycling Results

We have selected the LFP/LTO system to test this new design as it more established and stable than the LFP/Gr system. LTO anodes operate at a higher potential (~ 1.55 V vs. Li/Li^+) when compared to graphite (0.1 V vs Li/Li^+), which is within the stability window of most electrolytes. This higher operating potential results in less electrolyte decomposition and a thinner, less prominent SEI layer on LTO when compared to Gr anode. By starting with the more stable and long-lasting LFP/LTO system, we can more easily isolate and study the effects of new design elements, materials, or manufacturing processes without the confounding variables often present in LFP/Gr systems. The operating voltage for LFP/LTO chemistry is 1.8 V. The area occupied solely by the interdigitated electrode and interdigitated battlet electrode in each 1.8 V cell is 1.24 cm^2 and 1.20 cm^2

We first test the interdigitated structure to check the functioning of the co-planar design. Figure 4-5(a) and (b) show the charge and discharge curves at various C rates ($C/10$, $C/5$, $C/2$, $1C$, and $2C$) for interdigitated electrodes in organic (EC:DMC 1:1) and ionic liquid electrolyte (LiFSI:PYR14FSI 2:3) respectively. We do not use any additives here as the SEI formation is not a very critical factor in case of LTO anodes. No separator is used in the assembly as the electrodes are well separated. The cathode battlet interdigitated electrodes were 0.8 mg/cm^2 of loading density, which is equivalent to $0.1\text{--}0.11\text{ mAh/cm}^2$ of areal capacity (theoretical capacity of graphite 170 mAh/g). The first cycle coulombic efficiency in case the organic and ionic liquid electrolyte are 94.18% and 88.17% respectively. The cell with organic electrolyte showed a peak capacity of $>90\%$ of theoretical capacity and $\sim 80\%$ for the cell with ionic liquid electrolyte.

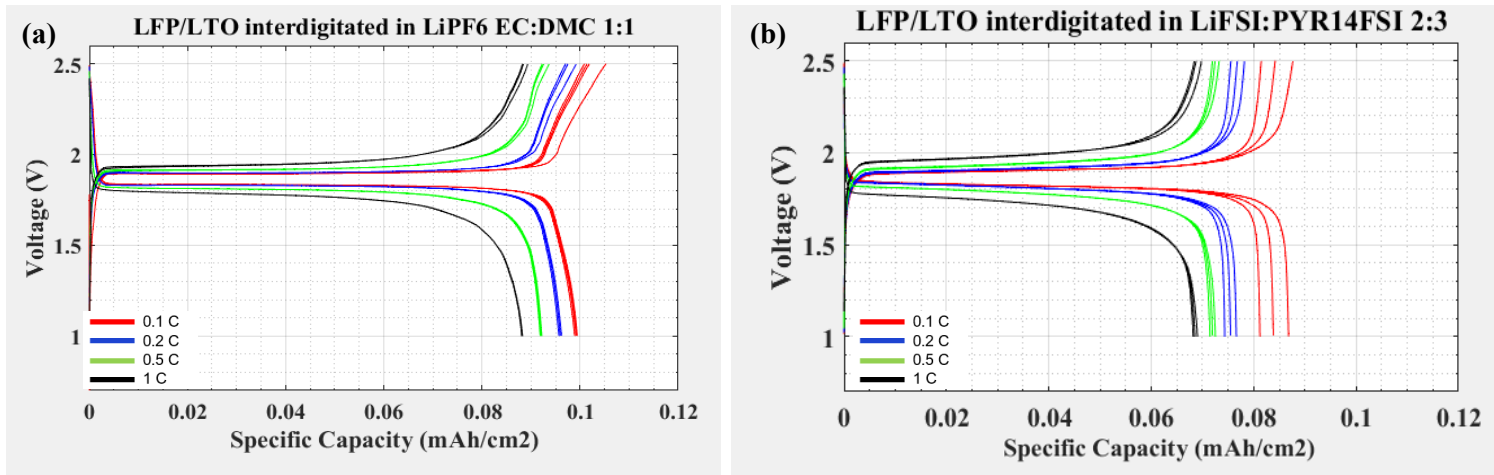


Figure 4-5: Charge/discharge cycle of LFP/LTO interdigitated battery in (a) organic electrolyte (b) ionic liquid electrolyte

For the interdigitated battlet electrode battery design testing cathode electrodes were of 0.77 mg/cm² loading density, which is equivalent to 0.1-0.11 mAh/cm² of areal capacity. Figure 4-6 (a) and (b) show the charge and discharge curves at various C rates for electrodes in organic (EC:DMC 1:1) and ionic liquid electrolyte (LiFSI:PYR14FSI 2:3) respectively. The first cycle coulombic efficiency in case the organic and ionic liquid electrolyte are 94.56% and 85.67% respectively. The cell with organic electrolyte showed a peak capacity of >90% and ~84% for the cell with ionic liquid electrolyte. The capacity drop at higher C-rates in the battlet interdigitated structure is more when compared to the interdigitated structure. This might be because larger area of current collector remains uncovered in this case.

When portions of the current collector remain uncovered by electrode materials, localized regions of elevated current density develop at the boundaries between coated and uncoated areas. This increases the effective electrical resistance over time and degrades cell stability [51]. One way to avoid this would be to cover the current collector with a carbon conductive layer which is generally used in current collector foils for conventional Li-ion batteries.

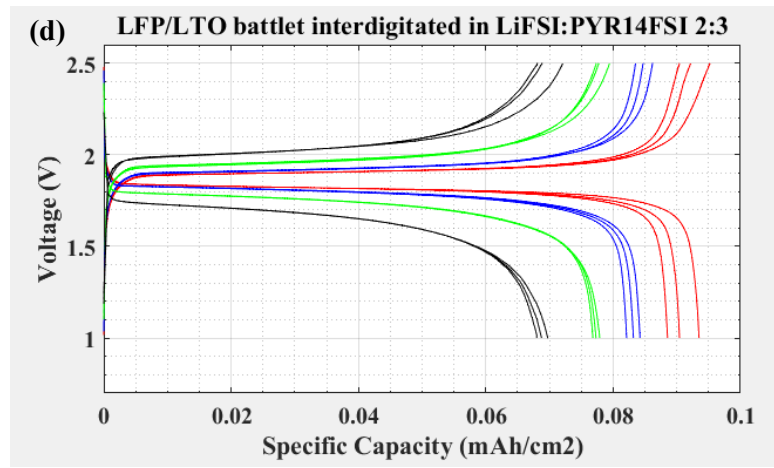
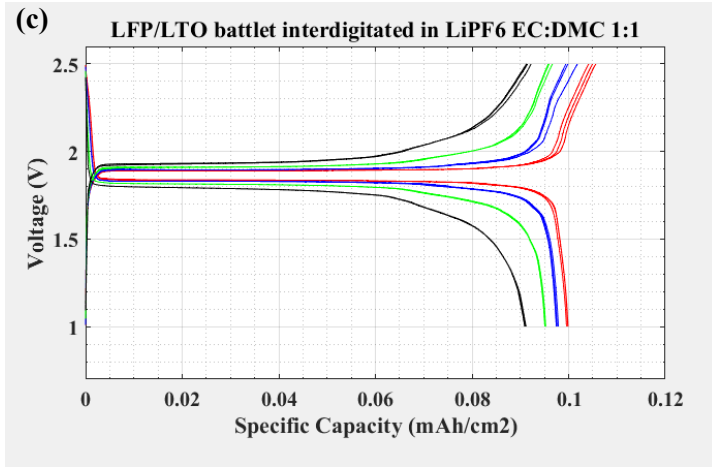


Figure 4-6: Charge/Discharge cycle of LFP/LTO battlet interdigitated battery in (a) organic electrolyte (b) ionic liquid electrolyte

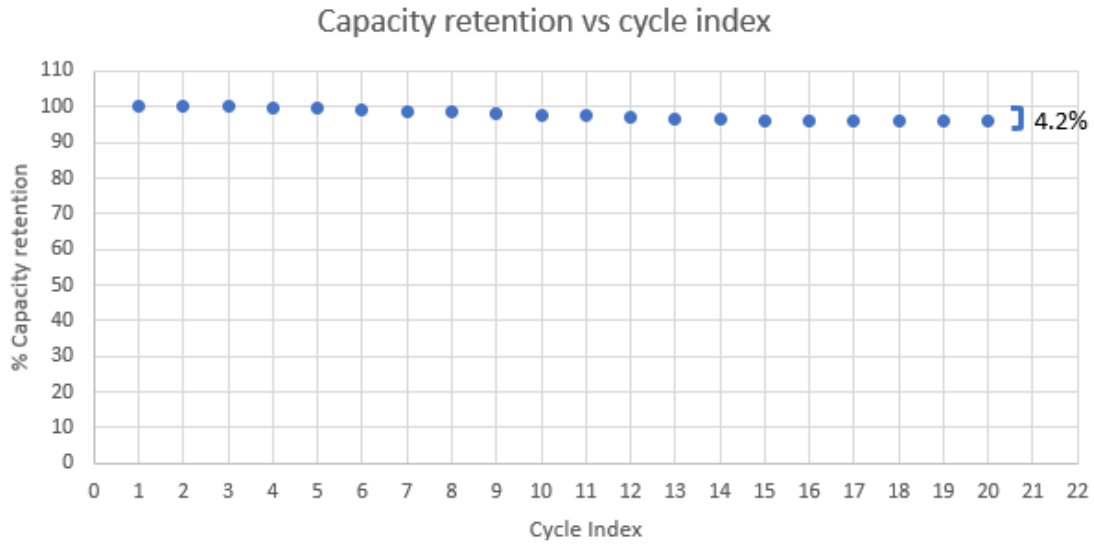


Figure 4-7: % capacity retention in LFP/LTO battlet interdigitated cell in ionic liquid electrolyte cycled at 0.2C over 20 cycles.

Figure 4-7 shows that the battlet interdigitated cell was able to maintain a reasonable capacity of 95.85% after 20 charge/discharge cycles at 0.2C. Therefore, in this work we have successfully fabricated a battlet interdigitated Li-ion battery on flexible biocompatible PDMS substrate which demonstrates $\sim 0.1 \text{ mAh/cm}^2$ of areal capacity at 0.1C delivering 1.8V. Figure 4-8 shows the packaged interdigitated battery after fully charging the it at 0.1C demonstrating stable voltage under dynamic bending. This demonstrates the functioning of a packaged interdigitated battlet flexible Li-ion battery on FlexTrateTM.

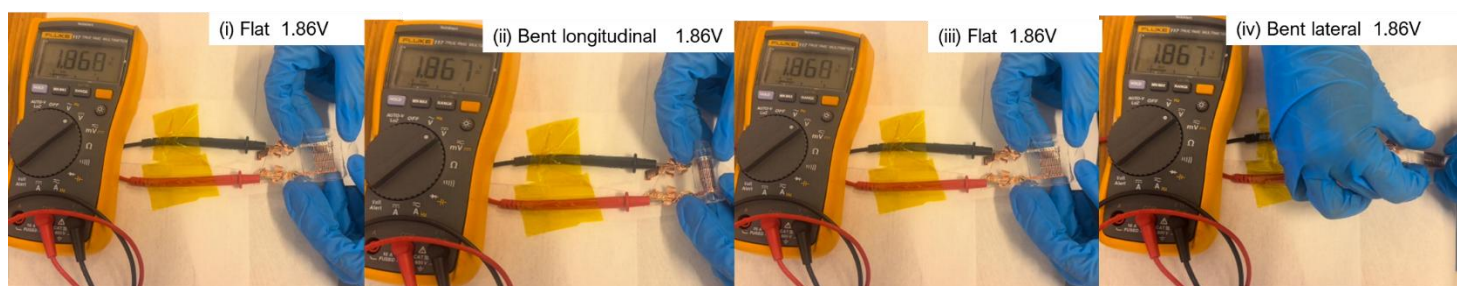
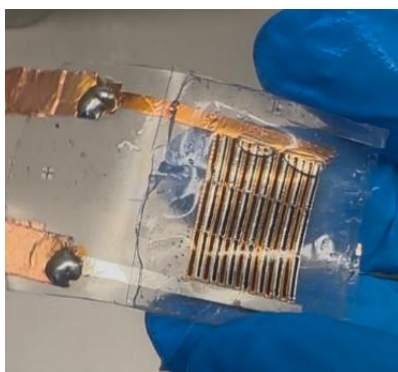


Figure 4-8: (a) Packaged battery (b) Dynamic Bending (5mm bending radius).

Here we showed that interdigitated electrodes of width 350-400 μm where the Li^+ diffusion length was 250-200 μm delivered 84% theoretical areal capacity in ionic liquid electrolyte with LFP/LTO chemistry. In case of a cofacial design electrode lower than 100 μm deliver lower % theoretical capacity, this demonstrates the benefits of using the coplanar design for developing flexible batteries with high energy per footprint. As the Li^+ diffusion distance is going to remain fixed as we increase the electrode height in the interdigitated coplanar design, as a part of the ongoing research, we will attempt to achieve higher areal capacity ($>1\text{mAh}/\text{cm}^2$) by printing thicker electrode ($>100\mu\text{m}$) using multilayer printing method in the ink-jet printer. We also aim to test the LFP/Gr chemistry in the battlet interdigitated design that delivers a higher voltage of 3.7V which is required for devices powering wearable devices.

CHAPTER 5: CONCLUSION AND FUTURE WORK

Flexible Li-ion batteries for flexible electronic devices are still in the early stages of development, particularly for high-capacity applications. In this thesis, we explored two design approaches to fabricate flexible Li-ion batteries using ionic liquid electrolytes, with a focus on powering wearable devices while ensuring safety and non-flammability. After optimizing the electrolyte properties, we demonstrated a peak capacity of 0.75 mAh/cm² (76% of the theoretical capacity of 1.2 mAh/cm²) for the LFP/Gr co-facial battery design, which operates at 3.7 V and withstands 1,000 bending cycles at a 5 mm bending radius.

This study revealed that high-concentration electrolyte (HCE) ionic liquid electrolytes inhibit solvent intercalation by reducing cation interaction in the solvation shell, leading to improved performance compared to low-concentration electrolyte (LCE) ionic liquid electrolytes. However, the cell performance remains limited by the high viscosity and lower conductivity of HCE electrolytes. One potential solution to reduce viscosity is the incorporation of a secondary solvent that does not coordinate with Li⁺ ions, forming a localized high-concentration electrolyte (LHCE) system [30]. Another alternative to enhance battery capacity is the use of tri-ethyl phosphate (TEP) as a solvent with LiFSI salt, which is non-flammable and exhibits lower viscosity compared to ionic liquid electrolytes.

To address the challenges of misalignment and Li⁺ diffusion limitations in the co-facial battery design, we developed a co-planar interdigitated battery design. This design delivers an areal capacity of 0.09 mAh/cm² at 1.8 V for LFP/ionic liquid electrolyte/ LTO cell chemistry, with an electrode width of 400 μ m (200 μ m Li⁺ diffusion length). The co-planar design demonstrates stable cycling at various C-rates, outperforming the co-facial design, which shows poor cycling performance at electrode thicknesses greater than 100 μ m.

In the next phase of this research, we will focus on conducting long-term bending tests to evaluate the mechanical and electrical reliability of the interdigitated structure in the bent state. Additionally, future work will involve optimizing slurry viscosity and ink-jet printing parameters to enable the printing of multilayer electrodes. This approach will increase the height of each electrode while keeping the width constant, thereby enhancing the loading density and areal capacity of the interdigitated electrode. Currently, the areal capacity is limited to 0.1 mAh/cm² at an electrode height of 30 μm. As shown in Figure 5-1, a four-layer LFP electrode printed using the ink-jet printer with a width of 370 μm and a height of approximately 110 μm, with each layer clearly distinguishable in the SEM image. Our goal is to achieve electrode thicknesses greater than 100 μm using ink-jet printing technology, which would yield an overall theoretical areal capacity of ≥ 1 mAh/cm².

Achieving this milestone will enable the fabrication of thin (<500 μm) flexible Li-ion batteries with non-flammable electrolytes, offering good capacity and electrochemical performance. Such batteries can be seamlessly integrated with wireless battery modules, physiological sensors, and signal processing subsystems on the same FlexTrate™ platform, forming a fully functional wearable device.

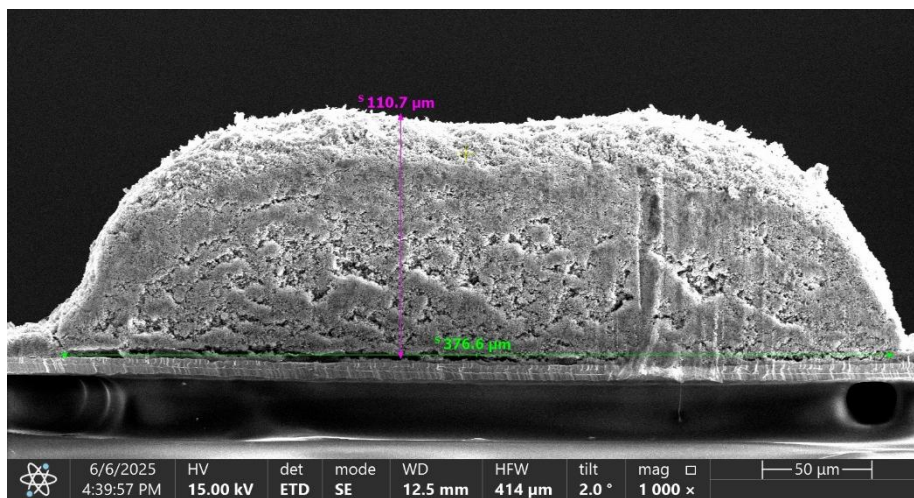


Figure 5-1: SEM image (1000x) of 4-layer LFP interdigitated electrode printed using direct-ink writing

REFERENCES

- [1] Li, J., Zhao, J., & Rogers, J. A. (2018). Materials and designs for power supply systems in skin-interfaced electronics. *Accounts of chemical research*, 52(1), 53-62.
- [2] Kim, Y. S., Mahmood, M., Lee, Y., Kim, N. K., Kwon, S., Herbert, R., ... & Yeo, W. H. (2019). All-in-one, wireless, stretchable hybrid electronics for smart, connected, and ambulatory physiological monitoring. *Advanced Science*, 6(17), 1900939.
- [3] Y. Liang et al., "A review of rechargeable batteries for portable electronic devices," *InfoMat*, vol. 1, no. 1, pp. 6–32, 2019, doi: 10.1002/inf2.12000.
- [4] T. K. Lee et al., "PEO based polymer electrolyte comprised of epoxidized natural rubber material (ENR50) for Li-Ion polymer battery application," *Electrochimica Acta*, vol. 316, pp. 283–291, Sep. 2019, doi: 10.1016/j.electacta.2019.05.143.
- [5] W. J. Chang et al., "Direct Observation of Carboxymethyl Cellulose and Styrene–Butadiene Rubber Binder Distribution in Practical Graphite Anodes for Li-Ion Batteries," *ACS Appl. Mater. Interfaces*, vol. 11, no. 44, pp. 41330–41337, Nov. 2019, doi: 10.1021/acsami.9b13803.
- [6] J. Li, R. B. Lewis, and J. R. Dahn, "Sodium Carboxymethyl Cellulose: A Potential Binder for Si Negative Electrodes for Li-Ion Batteries," *Electrochem. Solid-State Lett.*, vol. 10, no. 2, p. A17, Dec. 2006, doi: 10.1149/1.2398725.
- [7] "3D-Printed All-Fiber Li-Ion Battery toward Wearable Energy Storage - Wang - 2017 - *Advanced Functional Materials* - Wiley Online Library." Accessed: Feb. 19, 2022. [Online]. Available: <https://onlinelibrary.wiley.com/doi/full/10.1002/adfm.201703140> 99

- [8] A. Babapoor, M. Azizi, and G. Karimi, "Thermal management of a Li-ion battery using carbon fiber-PCM composites," *Appl. Therm. Eng.*, vol. 82, pp. 281–290, May 2015, doi: 10.1016/j.applthermaleng.2015.02.068.
- [9] J. Zhou et al., "A Quasi-Solid-State Flexible Fiber-Shaped Li–CO₂ Battery with Low Overpotential and High Energy Efficiency," *Adv. Mater.*, vol. 31, no. 3, p. 1804439, 2019, doi: 10.1002/adma.201804439.
- [10] L. Huang, Z. Zhang, Z. Wang, L. Zhang, X. Zhu, and D. D. Dorrell, "Thermal runaway behavior during overcharge for large-format Lithium-ion batteries with different packaging patterns," *J. Energy Storage*, vol. 25, p. 100811, Oct. 2019, doi: 10.1016/j.est.2019.100811.
- [11] E. Foreman et al., "A Review of Inactive Materials and Components of Flexible Lithium Ion Batteries," *Adv. Sustain. Syst.*, vol. 1, no. 11, p. 1700061, 2017, doi: 10.1002/adsu.201700061.
- [12] A. Balducci, "Ionic Liquids in Lithium-Ion Batteries," *Top. Curr. Chem.*, vol. 375, no. 2, p. 20, Feb. 2017, doi: 10.1007/s41061-017-0109-8. 100
- [13] H. Srour et al., "Ionic liquid-based electrolytes for lithium-ion batteries: review of performances of various electrode systems," *J. Appl. Electrochem.*, vol. 46, no. 2, pp. 149–155, Feb. 2016, doi: 10.1007/s10800-015-0905-1.
- [14] V. Nilsson, R. Younesi, D. Brandell, K. Edström, and P. Johansson, "Critical evaluation of the stability of highly concentrated LiTFSI - Acetonitrile electrolytes vs. graphite, lithium metal and LiFePO₄ electrodes," *J. Power Sources*, vol. 384, pp. 334–341, Apr. 2018, doi: 10.1016/j.jpowsour.2018.03.019.

- [15] X.-G. Sun and S. Dai, “Electrochemical investigations of ionic liquids with vinylene carbonate for applications in rechargeable lithium ion batteries,” *Electrochimica Acta*, vol. 55, no. 15, pp. 4618–4626, Jun. 2010, doi: 10.1016/j.electacta.2010.03.019.
- [16] A. Guerfi et al., “Improved electrolytes for Li-ion batteries: Mixtures of ionic liquid and organic electrolyte with enhanced safety and electrochemical performance,” *J. Power Sources*, vol. 195, no. 3, pp. 845–852, Feb. 2010, doi: 10.1016/j.jpowsour.2009.08.056.
- [17] Winter, M., Besenhard, J. O., Spahr, M. E., & Novak, P. (1998). Insertion electrode materials for rechargeable lithium batteries. *Advanced materials*, 10(10), 725-763.
- [18] Korthauer, R. (Ed.). (2018). *Lithium-ion batteries: basics and applications*. Springer.
- [19] Ling, JinKiong, et al. "Phosphate polyanion materials as high-voltage lithium-ion battery cathode: a review." *Energy & Fuels* 35.13 (2021): 10428-10450.
- [20] Winter M, Besenhard JO, Spahr ME, Novák P (1998) *Adv Mater* 10:725
- [21] Kim, E., Han, J., Ryu, S., Choi, Y., & Yoo, J. (2021). Ionic liquid electrolytes for electrochemical energy storage devices. *Materials*, 14(14), 4000.
- [22] A. Alam et al., “Heterogeneous Integration of a Fan-Out Wafer-Level Packaging Based Foldable Display on Elastomeric Substrate,” in 2019 IEEE 69th Electronic Components and Technology Conference (ECTC), Las Vegas, NV, USA: IEEE, May 2019, pp. 277–282. doi: 10.1109/ECTC.2019.00048.
- [23] G. Ouyang, G. Whang, E. MacInnis, and S. S. Iyer, “Fabrication of Flexible Ionic-Liquid Thin Film Battery Matrix on FlexTrate™ for Powering Wearable Devices,” in 2021 IEEE 71st Electronic Components and Technology Conference (ECTC), Jun. 2021, pp. 1620–1626. doi: 10.1109/ECTC32696.2021.00257.

- [24] Hildenbrand, F., Aupperle, F., Stahl, G., Figgmeier, E., & Sauer, D. U. (2022). Selection of electrolyte additive quantities for lithium-ion batteries using bayesian optimization. *Batteries & Supercaps*, 5(7), e202200038.
- [25] Markevich, E., Salitra, G., & Aurbach, D. (2017). Fluoroethylene carbonate as an important component for the formation of an effective solid electrolyte interphase on anodes and cathodes for advanced Li-ion batteries. *ACS Energy Letters*, 2(6), 1337-1345.
- [26] Swallow, J. E., Fraser, M. W., Kneusels, N. J. H., Charlton, J. F., Sole, C. G., Phelan, C. M., ... & Weatherup, R. S. (2022). Revealing solid electrolyte interphase formation through interface-sensitive Operando X-ray absorption spectroscopy. *Nature Communications*, 13(1), 6070.
- [27] Tong, J., Wu, S., Von Solms, N., Liang, X., Huo, F., Zhou, Q., ... & Zhang, S. (2020). The effect of concentration of lithium salt on the structural and transport properties of ionic liquid-based electrolytes. *Frontiers in chemistry*, 7, 945.
- [28] <https://solvionic.com/en/6-electrolytes?q=Sels-Li+FSI>
- [29] Salvador, M. A., Maji, R., Rossella, F., Degoli, E., Ruini, A., & Magri, R. (2023). Structural and Dynamic Characterization of Li-Ionic Liquid Electrolyte Solutions for Application in Li-Ion Batteries: A Molecular Dynamics Approach. *Batteries*, 9(4), 234.
- [30] Inhibiting Solvent Co-Intercalation in Graphite Anode by Localized High-Concentration Electrolyte in Fast-Charging Batteries
- [31] Takahashi, T., Ishikawa, M., Ugata, Y., Dokko, K., & Watanabe, M. (2021). Effects of Lithium Salt Concentration in Ionic Liquid Electrolytes on Battery Performance of LiNi_{0.5}Mn_{0.3}Co_{0.2}O₂/Graphite Cells. *Electrochemistry*, 89(5), 455-460.

- [32] Liu, X., Xu, C., Adenusi, H., Wu, Y., & Passerini, S. (2025). Development of PFAS-Free Locally Concentrated Ionic Liquid Electrolytes for High-Energy Lithium and Aluminum Metal Batteries. *Accounts of Chemical Research*, 3049-3057.
- [33] Haskins, J. B., Bennett, W. R., Wu, J. J., Hernández, D. M., Borodin, O., Monk, J. D., ... & Lawson, J. W. (2014). Computational and experimental investigation of Li-doped ionic liquid electrolytes:[pyr14][TFSI],[pyr13][FSI], and [EMIM][BF4]. *The Journal of Physical Chemistry B*, 118(38), 11295-11309.
- [34] Wang, H., Wu, C. H., Eren, B., Hao, Y., Feng, B., Fang, H. T., & Salmeron, M. (2019). Operando STM study of the interaction of imidazolium-based ionic liquid with graphite. *Energy Storage Materials*, 20, 139-145.
- [35] Liu, X., Mariani, A., Zarrabeitia, M., Di Pietro, M. E., Dong, X., Elia, G. A., ... & Passerini, S. (2022). Effect of organic cations in locally concentrated ionic liquid electrolytes on the electrochemical performance of lithium metal batteries. *Energy Storage Materials*, 44, 370-378.
- [36] Ouyang, G., Sheth, M., Sun, H., & Iyer, S. S. (2024, May). Integration of a Flexible Thin-Film Lithium-Ion Battery with a Wireless Charging System and a Flexible Micro-LED Array. In *2024 IEEE 74th Electronic Components and Technology Conference (ECTC)* (pp. 164-170). IEEE.
- [37] <https://analyticalscience.wiley.com/content/news-do/tracking-dendrites-destroy-batteries>
- [38] Li, D., Lv, Q., Zhang, C., Zhou, W., Guo, H., Jiang, S., & Li, Z. (2022). The effect of electrode thickness on the high-current discharge and long-term cycle performance of a lithium-ion battery. *Batteries*, 8(8), 101.

- [39] Xu, K., Zhao, N., Li, Y., Wang, P., Liu, Z., Chen, Z., ... & Liu, C. (2022). Design and 3D printing of interdigitated electrode structures for high-performance full lithium-ion battery. *Chinese Journal of Mechanical Engineering: Additive Manufacturing Frontiers*, 1(4), 100053.
- [40] Zhao, Y., & Guo, J. (2020). Development of flexible Li-ion batteries for flexible electronics. *InfoMat*, 2(5), 866-878.
- [41] Li, J., Zhao, J., & Rogers, J. A. (2018). Materials and designs for power supply systems in skin-interfaced electronics. *Accounts of chemical research*, 52(1), 53-62.
- [42] Zheng, S., Wu, Z. S., Zhou, F., Wang, X., Ma, J., Liu, C., ... & Bao, X. (2018). All-solid-state planar integrated lithium ion micro-batteries with extraordinary flexibility and high-temperature performance. *Nano Energy*, 51, 613-620.
- [43] Kim JS, Ko D, Yoo DJ, et al. A half millimeter thick coplanar flexible battery with wireless recharging capability. *Nano Lett.*2015;15(4):2350-2357
- [44] Liao, X., Shi, C., Wang, T., Qie, B., Chen, Y., Yang, P., ... & Yang, Y. (2019). High-energy-density foldable battery enabled by zigzag-like design. *Advanced Energy Materials*, 9(4), 1802998.
- [45] Song, Z., Ma, T., Tang, R., Cheng, Q., Wang, X., Krishnaraju, D., ... & Jiang, H. (2014). Origami lithium-ion batteries. *Nature communications*, 5(1), 3140.
- [46] Song, Z., Wang, X., Lv, C., An, Y., Liang, M., Ma, T., ... & Jiang, H. (2015). Kirigami-based stretchable lithium-ion batteries. *Scientific reports*, 5(1), 10988.
- [47] Weng, W., Sun, Q., Zhang, Y., He, S., Wu, Q., Deng, J., ... & Peng, H. (2015). A gum-like lithium-ion battery based on a novel arched structure. *Advanced Materials*, 27(8), 1363-1369.

- [48] Wang, Y., Chen, C., Xie, H., Gao, T., Yao, Y., Pastel, G., ... & Hu, L. (2017). 3D-printed all-fiber li-ion battery toward wearable energy storage. *Advanced Functional Materials*, 27(43), 1703140.
- [49] Xu, S., Zhang, Y., Cho, J., Lee, J., Huang, X., Jia, L., ... & Rogers, J. A. (2013). Stretchable batteries with self-similar serpentine interconnects and integrated wireless recharging systems. *Nature communications*, 4(1), 1543.
- [50] Fukushima, T., Alam, A., Wan, Z., Jangam, S. C., Pal, S., Ezhilarasu, G., ... & Iyer, S. S. (2017, May). “FlexTrateTM”—Scaled Heterogeneous Integration on Flexible Biocompatible Substrates Using FOWLP. In *2017 IEEE 67th Electronic Components and Technology Conference (ECTC)* (pp. 649-654). IEEE
- [51] Taheri, P., Mansouri, A., Schweitzer, B., Yazdanpour, M., & Bahrami, M. (2013). Electrical constriction resistance in current collectors of large-scale lithium-ion batteries. *Journal of The Electrochemical Society*, 160(10), A1731.